

The *Pthaladyns*: GTP Competitive Inhibitors of Dynamin I and II GTPase Derived from Virtual Screening

Luke R. Odell,^{†,||} Dian Howan,[†] Christopher P. Gordon,[†] Mark J. Robertson,[†] Ngoc Chau,[‡] Anna Mariana,[‡] Ainslie E. Whiting,[‡] Ruben Abagyan,[§] James A. Daniel,[‡] Nick N. Gorgani,[‡] Phillip J. Robinson,[‡] and Adam McCluskey^{*,†}

[†]Chemistry, The University of Newcastle, University Drive, Callaghan, NSW 2308, Australia, [‡]Cell Signaling Unit, Children's Medical Research Institute, The University of Sydney, 214 Hawkesbury Road, Westmead, NSW 2145, Australia, and [§]Department of Molecular Biology, The Scripps Research Institute, 10550 North Torrey Pines Road, TCP-28, La Jolla, California 92037. ^{||}Current address: Organic Pharmaceutical Chemistry, Department of Medicinal Chemistry, Uppsala Biomedical Centre, Uppsala University, Box 574, SE-751 23 Uppsala, Sweden.

Received April 10, 2010

We report the development of a homology model for the GTP binding domain of human dynamin I based on the corresponding crystal structure of *Dictyostelium discoideum* dynamin A. Virtual screening identified 2-[(2-biphenyl-2-yl-1,3-dioxo-2,3-dihydro-1*H*-isoindole-5-carbonyl)amino]-4-chlorobenzoic acid (**1**) as a ~170 μ M potent inhibitor. Homology modeling- and focused library-led synthesis resulted in development of a series of active compounds (the “*pthaladyns*”) with 4-chloro-2-(2-(4-(hydroxymethyl)phenyl)-1,3-dioxoisindoline-5-carboxamido)benzoic acid (**29**), a $4.58 \pm 0.06 \mu$ M dynamin I GTPase inhibitor. *Pthaladyn-29* displays borderline selectivity for dynamin I relative to dynamin II (~5–10 fold). Only *pthaladyn-23* (dynamin I IC_{50} $17.4 \pm 5.8 \mu$ M) was an effective inhibitor of dynamin I mediated synaptic vesicle endocytosis in brain synaptosomes with an IC_{50} of $12.9 \pm 5.9 \mu$ M. This compound was also competitive with respect to $Mg^{2+} \cdot GTP$. Thus the *pthaladyns* are the first GTP competitive inhibitors of dynamin I and II GTPase and may be effective new tools for the study of neuronal endocytosis.

Introduction

Our laboratory has reported the identification and development of a number of discrete families of small molecule inhibitors of the large GTPase, dynamin I. The MitMABs,^{a,1,2} the Bis-Ts,^{3,4} the RTILs,⁵ the dynoles,⁶ and most recently, the iminodins exemplify these inhibitor families.⁷ Other groups have reported dynasore,⁸ and some selective serotonin reuptake inhibitors as dynamin inhibitors.⁹ None of these compounds bind to the active site (i.e., none are $Mg^{2+} \cdot GTP$ competitive). Without exception, all inhibitors have been discovered by biological assay-directed screening of chemical libraries, and in those instances where lead development has ensued, synthesis has been via focused library development.

To date, there has been no computer assisted molecular modeling-led development of dynamin inhibitors. This is in part due to the complex nature of dynamin, the multiple

potential drug targets within a molecule which has multiple domains, and the lack of a published structure to guide such efforts. No full dynamin crystal structure has been published, but there are now two known structures of individual domains (below). The three classical dynamins, dynamins I, II, and III, are large GTPases of approximately 100 kDa. All members of the dynamin superfamily include a GTPase domain, a GTPase effector domain (GED), and a middle domain, while some include a transmembrane region. The classical dynamins differ from others by two additional structural domains; a pleckstrin homology (PH) domain and a C-terminal proline-rich domain (PRD). Each of these five primary domains has distinct properties allowing dynamin to have multiple functions and subcellular locations.

The PH domain binds lipids such as phosphoinositide bisphosphate (PtdIns(4,5)P₂ or PIP₂) and is essential for dynamin localization and can promote a massive increase in GTPase activity by acting as a template for dynamin helical self-assembly.^{10,11} Both X-ray and NMR approaches have been used to solve the structure of this domain.^{12–16} The PH domain of dynamin I comprises a seven-stranded β -sheet sandwich, three variable loops, and a C-terminal α -helix. Site directed mutagenesis highlights K535 in variable loop 1 and variable loop 3 as essential for lipid binding and transferin endocytosis, and the K558E mutation in variable loop 3 causes the human neurodegenerative disease Charcot–Marie–Tooth.¹⁷ Thus the variable loops in the PH domain play pivotal roles in mediating dynamins lipid and membrane interactions.

The middle domain displays no homology with any known structural motif. Little is known about its role or function, although recent evidence indicates that middle domain

*To whom correspondence should be addressed. Phone: +61 249 216486. Fax: +61 249 215472. E-mail: Adam.McCluskey@newcastle.edu.au.

^a Abbreviations: RME, receptor mediated endocytosis; SVE, synaptic vesicle endocytosis; CME, clathrin-mediated endocytosis; GED, GTPase effector domain; PRD, proline rich domain; PH, Pleckstrin homology; SH3, Src homology 3; CMT, Charcot–Marie–Tooth disease; CNM, centronuclear myopathy; MitMAB, myristoyl trimethyl ammonium bromide; OctMAB, octyl trimethyl ammonium bromide; Bis-T, Bis-tyrphostin; RTIL, room temperature ionic liquid; SAR, structure–activity relationship; EGFR, epidermal growth factor receptor; Tf-TxR, Texas Red-Tf; U2OS, human bone osteosarcoma epithelial cells; PS, phosphatidylserine; PMSF, phenylmethylsulfonylfluoride; PFA, paraformaldehyde; FCS, fetal calf serum; DMEM, Dulbecco's Modified Eagle Medium; DMSO, dimethylsulfoxide; IXM, Image Xpress Micro; HEPES, 4-(2-hydroxyethyl)-1-piperazineethane sulfonic acid; FM 4-64, *N*-(3-triethylammoniumpropyl)-4-(4-diethylaminophenyl)hexatrienylpyridinium dibromide.

mutations in dynamin II may play a role in dominant centronuclear myopathy, a degenerative muscle wasting disease.¹⁸ The middle domain of dynamin II has also been shown to bind γ -tubulin, suggesting a role in centrosome cohesion.¹⁹

The GTPase domain is the site of GTP binding and hydrolysis and is the most highly conserved domain in the superfamily. It is characterized by an unusually low affinity for GTP (10–25 μ M), high rates of hydrolysis (1–20 min⁻¹), and extremely high turnover rates relative to other families of GTPases.^{20,21} Dynamin also has the unique ability (among GTPases) to self-assemble into macromolecular entities that stimulate basal GTPase activity up to 1000-fold.¹⁰ The dynamin superfamily GTPase domain structure grossly resembles that of other GTPases, with an eight-stranded β -sheet with six parallel and two antiparallel strands surrounded by nine helices.²²

Our interest in dynamin stems from the need to understand dynamin biology and recognition of the potential therapeutic implications associated with inhibiting a protein that is essential to the endocytotic machinery.^{23–25} All cells endocytose, it is the process whereby key cellular materials are taken up, the process by which synaptic vesicles are recycled; it is crucial for cell, and thus host survival.²⁶ But the molecular machinery deployed by cells to internalize plasma membrane varies according to task, which can range from nutrient absorption to cell signaling. Dynamin does not mediate all forms of endocytosis, but its action includes clathrin-mediated endocytosis (CME). Clathrin-mediated endocytosis is a dynamic biological process requiring logistically complex assembly and utilization of numerous specialized protein and lipid complexes. *Synaptic vesicle endocytosis* (SVE) is a neuronal endocytic specialization that facilitates the recovery of synaptic vesicles after membrane fusion and neurotransmitter release (exocytosis) and involves at least two dynamin-dependent modes, CME and bulk endocytosis.²⁷ *Receptor mediated endocytosis* (RME) is initiated on activation of surface bound receptors (via endogenous ligand binding) and is the primary vehicle for cells to uptake membrane material.²⁸ Of the known forms of endocytosis, clathrin-induced membrane deformation to form nascent vesicles is the most fully understood.²⁹ Clathrin typically recruits membrane proteins (multimeric adaptor proteins, AP-2).³⁰ This assists in the development of an almost fully closed invaginated vesicle but requiring the protein dynamin to detach the vesicle from the membrane. In this final step, GTP hydrolysis by dynamin appears to supply the energy to release the vesicle from the membrane. Dynamin is involved at this point by targeting to sites of endocytosis via its PH domain and then stimulating its GTPase activity.³¹ There are numerous potential avenues for clinical application of dynamin inhibitors in the future. One possibility is their use as potential antiepileptic drugs due to their ability to produce a run-down in synaptic transmission as a result of inhibiting SVE.³² Their ability to block the function of dynamin II in cytokinesis raises the possibility of their application as new antimitotic agents.³³ Their ability to block HIV entry into cells implies a potential future application in the treatment of infectious diseases.³⁴

While we have discovered and developed a large “palette” of small molecule inhibitors of dynamin that target distinct domains,^{1–7} none yet display GTP competitive kinetics, indicative of binding at the active site of dynamin. Therefore our goal is to impart our dynamin modulators program with a degree of rational drug design by development of a dynamin GTPase domain homology model with a view to conducting a

virtual screening program to identify new dynamin inhibitors. The model can then be used to guide the subsequent rational design of more potent inhibitors. This is not a new approach, with known crystal structures and cocrystals virtual library screening becoming an increasingly important tool in the discovery of novel and diverse lead structures.^{35,36} Virtual library screening has recently successfully identified new lead compounds for a host of different biological targets including: protein kinase inhibitors,³⁷ reverse transcriptase of human immunodeficiency virus type-1,³⁸ glutamate receptor agonists,³⁹ dengue virus methyltransferase,⁴⁰ proteasome inhibitors,⁴¹ and falcipain-2 inhibitors as potential antimalarial agents.⁴² We sought to utilize a structure based screening approach in the discovery of novel dynamin inhibitors that may target the nucleotide binding pocket for the first time. Herein, we describe the generation and validation of a homology model of the human dynamin I GTPase domain and the subsequent library development of novel dynamin inhibitors that we have called the “phtaladyns”.

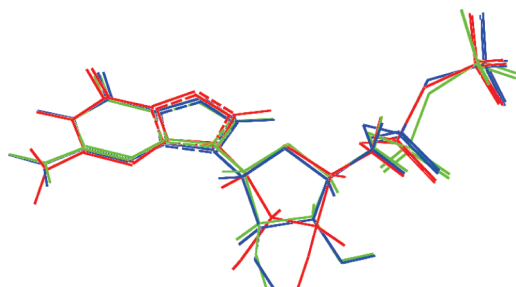
Results and Discussion

It is well established that reasonable structural models can be constructed when a 3D template and target protein share greater than 30% sequence identity.⁴³ A pairwise sequence alignment between the GTPase domains of dynamin I and dynamin A revealed a 64% sequence identity. Dynamin I, like all GTPases, has four consensus elements (G1–G4) which are involved in nucleotide binding. The sequence identity between the two proteins reaches 89% when the 18 residues forming the nucleotide-binding site are examined.⁴⁴ Consequently, we were confident that an accurate structural model for the dynamin I GTPase domain that included the nucleotide binding pocket could be constructed utilizing dynamin A as a template. The G2 motif, a Mg²⁺ coordinating flexible loop, was not resolved in the crystal structure of dynamin A and represented a potential limitation in the construction of our dynamin I homology model. Notwithstanding this, other crucial residues were expected to allow excellent alignment and hence we anticipated that a homology model of the GTPase domain of dynamin I suitable for ligand database screening would eventuate.

We constructed seven different models via ICM homology (ICM v3.1) based on the GDP bound structure of the dynamin A GTPase domain (PDB code 1JWY) (for details see Experimental Section).⁴⁵ To include ligand information in our models, GTP was docked onto a grid representation of the nucleotide-binding site and the best solutions refined using a full atom representation of the binding site. GTP and GDP were then redocked onto a grid representation of the refined nucleotide-binding sites, and their ICM scores were evaluated (Table 1). The ICM-score takes into account the ligand–receptor interaction energy, conformational strain energy of the ligand, conformational entropy loss, and desolvation effects.⁴⁶ The score reflects the overall quality of the ligand–receptor complex with a more negative score indicating a more favorable interaction (Table 1). Two of the proposed structures (hDyn1–3 and hDyn1–7) showed greater predicted binding affinity than the other models (e.g., GTP –79.13 and –79.87, respectively, vs –68.76). In addition, their ICM scores were lower for GDP than GTP (–75.55 and –71.51 vs –79.13 and –79.87, respectively), consistent with dynamin’s known lower affinity for GDP.⁴⁷ Accordingly, these two structures were selected for further validation studies.

Table 1. Homology Model Representations and Their ICM Scores for the Interaction with GDP and GTP

model	ICM score	
	GDP	GTP
hDyn1-1	-60.87	-29.75
hDyn1-2	-64.85	-39.95
hDyn1-3	-75.55	-79.13
hDyn1-4	-67.60	-68.76
hDyn1-5	-69.08	-73.39
hDyn1-6	-65.32	-49.17
hDyn1-7	-71.51	-79.87

**Figure 1.** Binding modes of GDP predicted using hDyn1-3 (red) and hDyn1-7 (green) relative to the conformation found in the dynamin A crystal structure (blue, PDB code 1JWY).

To validate our models, GDP was docked in the modeled structures using the ICM flexible ligand-grid receptor algorithm and the predicted ligand pose was compared to the crystal structure conformation. Each of the models was able to effectively reproduce the crystal structure conformation with rmsd's of 0.69 and 0.77 Å for hDyn1-3 and hDyn1-7, respectively (rmsd < 2 Å is considered accurate),⁴⁸ thus illustrating the accuracy of our predicted binding site representations (Figure 1).

The stereochemical properties of the hDyn1-3 and hDyn1-7 models were assessed and found to be within acceptable limits (PROCHECK).⁴⁹ The Ramachandran plot showed that, in both models, 84.5% of the residues are located within the core region, 13.2% in the allowed and 2.3% in the generously allowed regions. Additionally, checks for bond lengths, side chain torsions, amide torsions, and backbone torsions showed no major deviations from the allowed values. Only 5.2% of residues showed bond angles with higher than expected values (> 4.4 standard deviations), however, these residues were not located within the nucleotide-binding site and accordingly were deemed less relevant to this study. These analyses show that our homology models are not only consistent with current understanding of protein structure but are also able to accommodate GTP in a native conformation.

During the completion of this work, the *apo* crystal structure of the GTPase domain of *Rattus norvegicus* dynamin I was solved and this protein shares a 99.3% sequence identity with the human dynamin I GTPase domain.⁵⁰ Thus, our modeled structures could be validated retrospectively by comparison to the solved structure (Figure 2). hDyn1-3 and hDyn1-7 have rmsd's of 1.09 Å for C α atoms and 1.74 and 1.79 Å for all heavy atoms, respectively, when compared to the crystal structure. Furthermore, the GTP binding residues in hDyn1-3 and hDyn1-7 have heavy atom rmsd's of 0.71 and 0.70 Å, respectively, when compared to the same residues in the crystal structure. These results confirmed the accuracy of our models and their relevance in further ligand docking studies. Although these structures are invaluable

**Figure 2.** Backbone structure of homology models hDyn1-3 and hDyn1-7 (red) superimposed (C α rmsd 1.09 Å) on the rat dynamin I GTPase domain crystal structure (green, PDB code 2AKA).

within a drug design program, essentially allowing a medicinal chemist to custom build ligands, a significant limitation of currently available molecular docking software is that the enzyme effectively remains static throughout a simulation. Given the dynamic ligand-enzyme binding interactions that typically occur in vivo, an understanding of the potential movements and flexibility of the target enzyme is extremely valuable in the assessment and validation of docking results. To assess potential flexibility of the dynamin, GTPase-GDP cocrystallized structure (1JWY) and the ligand free structure (1JX2) were compared utilizing the PROFLEX program. This revealed that the conformation of the crystal structures deviated significantly (> 8 Å) in two regions, specifically the side-chains of residues 152-156 and 252-254 (see Supporting Information). Consequently, docked conformations in close proximity to either of these flexible regions would need to be assessed with a degree of caution.

Flexible ligand and receptor docking is still far too computationally expensive to be considered viable for large database screening, e.g. ~800000 compounds (ChemBridge, San Diego, CA, and ChemDiv, San Diego, CA). To achieve this goal in a reasonable time frame and to account for some receptor flexibility, we used both homology model representations (hDyn1-3 and hDyn1-7) and the ICM flexible ligand-grid receptor algorithm for virtual ligand screening. The flexible ligands passing a relaxed Lipinski filter (MW < 600, HBA < 12, and HBD < 6) and containing less than seven rotatable bonds were docked into grid receptor field and ranked according to the scoring function implemented in ICM.⁵¹ The solutions from each receptor were merged and the top ranked 1000 compounds were considered potential inhibitors and clustered into diverse sets according to chemical similarity. Each compound, docked into the nucleotide-binding site, was visually inspected, and those displaying unfavorable interactions within the binding site or significant interactions with the G2 consensus region were discarded. To ensure diversity in the final compound selection, only 1-2 compounds from each cluster were retained. Finally, 300 compounds were requested from the vendors, of which 175 were still available for biological evaluation. The available compounds were submitted for initial biological

evaluation against in vitro dynamin I GTPase activity at two concentrations, 30 and 300 μM using methods described previously.¹ Compound **1** (Figure 3) was identified as a ~ 170 μM inhibitor of the GTPase activity of full length endogenous sheep brain dynamin I.

Considering dynamins' affinity for GTP is 10–25 μM the level of potency displayed by compound **1** was encouraging.²¹ While only a moderate dynamin inhibitor, the structural simplicity and ease of access to discrete libraries appealed, so we set about the development of **1** as a potential new class of dynamin I GTPase inhibitor. Retrosynthetic analysis of **1** revealed that preparation could occur via two straightforward condensation reactions from commercially available precursors (Figure 4). The inherent simplicity of this process struck us as amenable to rapid analogue development and the generation of SAR data. Moreover, the predicted binding mode of **1** in the active site could be used to guide analogue development.

Compound **1** fits well into the GTP binding site of dynamin, showing several hydrogen bonding, ionic, and van der Waals interactions with the active site residues (Figure 5). The acid group forms a salt bridge with the Lys44 side chain and also accepts hydrogen bonds from the backbone amide hydrogens of Ala42, Gly43, and Lys44. The amide carbonyl acts as a hydrogen bond acceptor with the Ser45 –OH, while the amide hydrogen donates a hydrogen bond to the Ser45 oxygen. In addition, the aromatic ring makes van der Waals contacts with the Ile63 side chain. The imide carbonyls can accept hydrogen bonds from the side chain hydrogens in Glu239 and Ser46. The phenyl group adjacent to the imide appears to make van der Waals interactions with the Lys206 and Val235 side chains. The additional 2-phenyl substituent appears to make van der Waals contacts with the Leu209 side chain.

This fitting revealed two factors pertinent to analogue development. First, the 1-amido-2-benzoic acid moiety makes a number of significant hydrogen bonding and ionic interactions within the binding site. These interactions appear to mimic that of phosphate groups in GTP and GDP, suggesting they may be crucial to the activity exhibited by compound **1**.

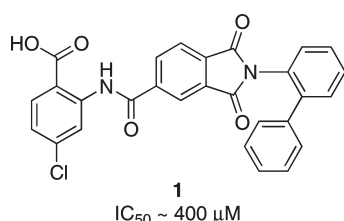


Figure 3. Chemical structure of pthalodyn-**1** identified by virtual screening of the Chembridge and ChemDiv screening databases.

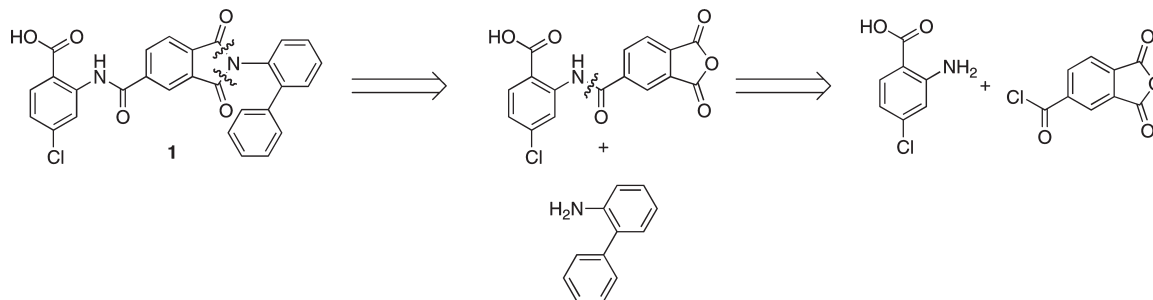


Figure 4. Retrosynthetic analysis of pthalodyn-**1** showing that preparation can occur via two condensation reactions from commercially available precursors.

Second, the 2-phenyl substituent is largely solvent exposed and makes only minimal van der Waals interactions with Leu209. Thus, its removal was not expected to significantly reduce potency, allowing a straightforward examination of the effect of additional aromatic ring substituents via a raft of simple commercially available anilines. Moreover, the binding site residues in this region (Asp208, Asn236, Arg237, Ser238, and Gln239) contain a number of potential hydrogen and ionic bond forming groups (CONH, OH, CONH₂, NH₂, C(NH)₂NH₂, COOH), which may interact with any complementary groups (i.e., OH, NH₂, COOH) introduced into our analogues (Figure 4). Therefore, we decided to prepare two discrete libraries of analogues to explore these factors, concurrent with the synthesis of **1**.

The strategy used in the synthesis of *Library A*, which explores the 1,2-amidobenzoic acid moiety is illustrated in Scheme 1. Synthesis commenced with the treatment of an excess of trimellitic anhydride chloride with the appropriately substituted aniline at 0 °C, to minimize the competing anhydride reaction.⁵² Compounds **5** and **7** could be isolated as the desired acid chloride adducts via crystallization and basic aqueous workup, respectively, however **4**, **6**, and **8** could not be purified in this manner and decomposed (presumably via anhydride opening) when flash column chromatography was attempted. Consequently, these compounds were used in the next step, without purification, as crude mixtures containing

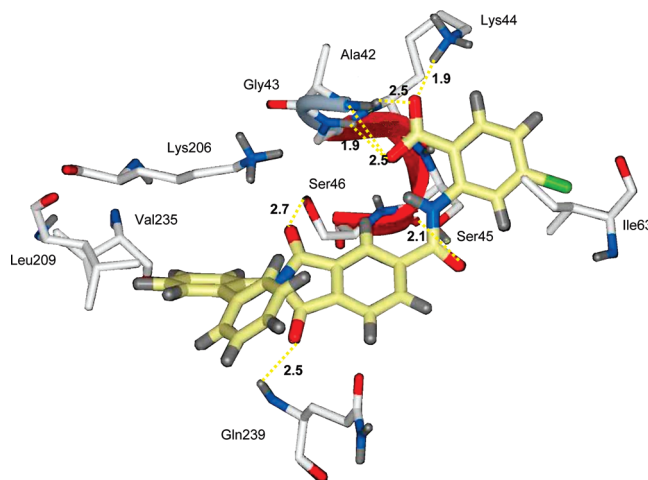
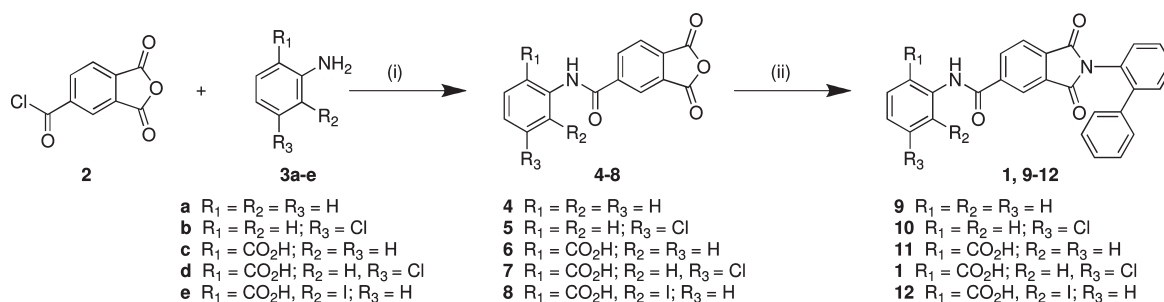
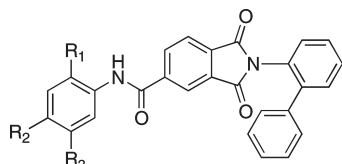


Figure 5. Predicted binding pose of compound **1** within the binding site of hDyn1–3. Color codes: oxygen, red; nitrogen, blue; hydrogen, gray; chlorine, green (for clarity only polar binding site hydrogen atoms are shown). Carbon atoms are shown in white (hDyn1–3) and yellow (**1**). Hydrogen bonds are shown as yellow dotted lines with atom distances in Å.

Scheme 1^a

^a Reagents and conditions: (i) THF, 0 °C, 3 h; (ii) 2-phenylamine, DMF, toluene, TEA, 130 °C, 18 h.

Table 2. Inhibition of Dynamin I GTPase Activity by Phthaladyns **1**, and **9–12**



Library A

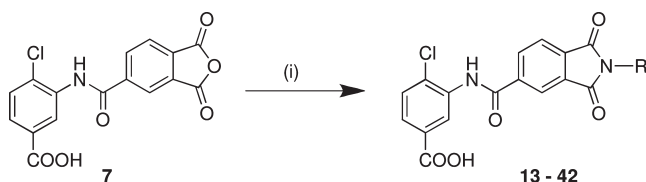
no.	R ₁	R ₂	R ₃	IC ₅₀ (μM)
1	COOH	H	Cl	> 400 ^a
9	H	H	H	
10	H	H	Cl	
11	COOH	H	H	
12	COOH	I	H	

^a ~40% inhibition at 400 μM.

ca. 80–90% (by ¹H NMR) of the desired acid chloride adducts. Treatment of **4–8** with biphenyl-2-ylamine in the presence of triethylamine (TEA) at 130 °C afforded the desired **1, 9–12** in moderate (40–70%) yields. We call this series the “*phthaladyns*” — phthalimide-based inhibitors of dynamin.

Library A comprised of five analogues which were evaluated for their ability to inhibit dynamin and this data is presented in Table 2. The most striking feature of Table 2 is that our in-house synthesized version of **1** displayed significantly weaker inhibitory activity than the vendor supplied compound (IC₅₀ ~ 170 vs > 400 μM (40% inhibition at 400 μM)). This may be the result of an error in the original assay or an error relating to vendor supply. Since completion of this work, we have obtained another sample of **1** from the vendor and its IC₅₀ correlated well with our synthesized version (IC₅₀ for both > 400 μM). While a poor lead, **1** was still predicted to have a GTP competition mechanism of action against dynamin (Figure 5), providing us with a compelling reason to continue with molecular modelling-led focused library generation. To date, no GTP competitive inhibitors of dynamin have been reported. Additionally, the SAR is consistent with the predicted role of the carboxylic acid in mediating active site binding and suggests that an electron-withdrawing group, preferably *para* to the acid, is also beneficial for inhibition.

We next set about developing SAR associated with the biaryl moiety via modeling guided synthesis of *Library B*. In our initial modeling analysis, we noted that the biphenyl moiety of **1** is encapsulated within a cavity defined by Lys206, Val235, and Leu209 (Figure 5). From these interactions, we believed

Scheme 2^a

^a Reagents and conditions: (i) RNH₂, DMF, toluene, TEA, 130 °C, 18 h.

that removal of the second phenyl ring would generate a phthaladyn with reduced activity but with sufficient space for later introduction of a range of substituents capable of better engagement with the aforementioned residues while at the same time removing the noted van der Waals interactions. Closer examination of this cavity reveals the presence of Asp208 that might be accessible with the appropriate choice of aromatic substituent, as are Asn236 and Ser238 on the cavity periphery.

Treatment of phthalic anhydride (**7**) with the appropriate aniline (Scheme 2, and see Table 3 for details) in the presence of TEA at 130 °C afforded the desired *Library B* constituents, **13–33** in low (**33**: 7%) to excellent (**18**: 84%) yields.

Synthesis and evaluation of the “naked” aniline analogue (**13**) gave, as anticipated, reduced biological activity (Table 3). With the compound skeleton in place, we rationalized that the Asp208 carboxylate was in sufficiently close proximity to interact with an amino moiety, thus we synthesized the 2-, 3-, and 4-NH₂ phthaladyn analogues **14–16**, respectively. Introduction of, in particular, the 3-NH₂ (**15**) gave rise to a significant increase in dynamin inhibition with an IC₅₀ value of 94 μM (Table 3). Both the 2- and 4-NH₂ analogues (**14, 16**) returned significantly lower levels of dynamin inhibition, returning IC₅₀ values of 311 ± 28 and > 400 μM, respectively. On the basis of these findings, a series of simple bioisosteric replacements were undertaken. The first resulted in the introduction of an –OH moiety, which was expected to hydrogen bond with Asp208. Gratifyingly, we note an increase in dynamin inhibition with the 2- and 4-OH analogues (**17** and **19** with IC₅₀ values of 61 ± 30.0 and 40 ± 10.0 μM, respectively). This increase in dynamin I inhibition was > 10 fold relative to **1** and can be attributed, in our model, to an additional hydrogen bond interaction, with the Asp208 side chain carbonyl accepting a hydrogen bond from the inhibitor OH group. Our preliminary modeling analysis suggests that the Asp208 side chain carbonyl accepts a hydrogen bond from **19**’s 4-OH group. “Methylation” of **18**’s and **19**’s phenolic OH gave **20** and **21**, of which only the 4-OCH₃ analogue (**21**) retained, albeit at a reduced level, dynamin inhibition with an IC₅₀ value of

Table 3. Inhibition of Dynamin I GTPase Activity by Pthaladyns 13–33

Library B

no.	R ₁	R ₂	R ₃	IC ₅₀ (μM)
13	H	H	H	<i>a</i>
14	NH ₂	H	H	311 ± 28
15	H	NH ₂	H	94
16	H	H	NH ₂	<i>a</i>
17	OH	H	H	61 ± 30
18	H	OH	H	<i>a</i>
19	H	H	OH	39.8 ± 10.0
20	H	OCH ₃	H	<i>a</i>
21	H	H	OCH ₃	78 ± 10.0
22	H	H	SCH ₃	<i>a</i>
23	H	NO ₂	H	17.4 ± 5.8
24	H	H	NO ₂	16.6 ± 7.0
25	CO ₂ H	H	H	184 ± 84
26	H	H	CO ₂ H	95
27	CH ₂ OH	H	H	<i>a</i>
28	H	CH ₂ OH	H	111
29	H	H	CH ₂ OH	4.58 ± 0.06
30	H	H	CO ₂ Et	<i>b</i>
31	H	H	CH ₂ CO ₂ H	95.5 ± 17.5
32	H	H	CH ₂ CH ₂ CO ₂ H	104
33	H	OH	CO ₂ H	267 ± 0.1

^a No activity observed at 400 μM. ^b ~50% inhibition at 300 μM.

78 ± 10.0 μM. This is consistent with the removal of the hydrogen bond donating capability of an –OH but retention of the hydrogen bond accepting capability. The 4-SCH₃ analogue (**22**) is inactive.

Next, we turned our attention to the possibility of better engaging additional residues on the periphery of the binding cavity and rationalized that the introduction of a –NO₂ moiety may allow hydrogen bond donation from Asp208 and also interactions with Asn236 and possibly Ser238. Both the 3-NO₂ (**23**), and 4-NO₂ (**24**) returned the highest levels of dynamin inhibition thus far observed with IC₅₀ values of 17.4 ± 5.8 and 16.6 ± 7.0 μM, respectively. Interestingly, the 2-CO₂H (**25**) and 4-CO₂H (**26**) displayed disappointing levels of dynamin inhibition, with IC₅₀ values of 184 ± 84 and 95 μM, respectively. This is presumably due to the more restricted matching conformation required to properly align both the pthaladyn –CO₂H and the Asp208 –CO₂H moieties. Indeed, re-examination of the binding pose of **26** clearly shows that the Asp208 –CO₂H twists so as to accommodate **26**'s –CO₂H moiety but in doing so the extent of favorable overlap is reduced, leading to a concomitant reduction in potency (Figure 6A,B). Pthaladyn **26**'s –CO₂H moiety is predicted to accept hydrogen bonds from the Asn236 backbone amide proton and the Ser238 side chain OH (Figure 6B). It is possible that these additional binding site contacts counteract the impact of a reduction in interaction with Asp208.

To better engage with Asp208 (Figure 6A), we sought to extend the H-bonding moiety closer to this amino acid, as we have seen that direct interaction results in a rotation of Asp208, but believed that the increased bulk of the CH₂

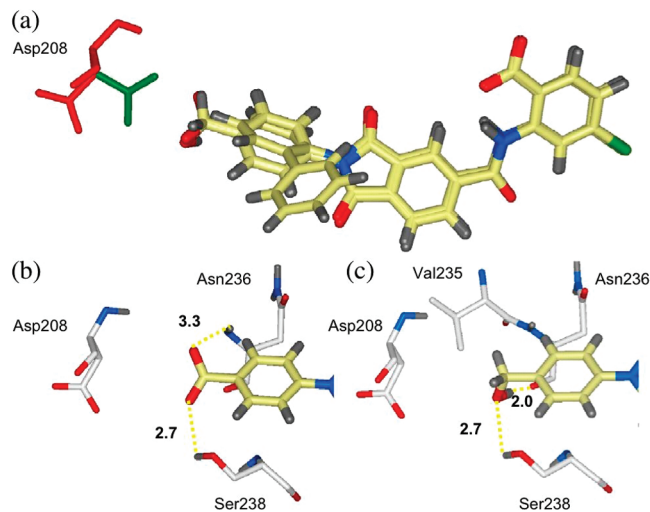


Figure 6. (a) Overlay of the predicted binding poses of compounds **1**, **26**, and **29** in the hDyn1–3 model. The Asp208 side chain has twisted and rotated to accommodate the bulkier acid and methanol groups in **26** and **29**. The original position is shown in green and the new position in red. (b) Predicted binding interactions of the acid group in compound **26**. (c) Predicted binding interactions of the CH₂OH group in compound **29**. Color codes: oxygen, red; nitrogen, blue; hydrogen, gray (for clarity only polar binding site hydrogens are shown). Carbon atoms are shown in white (hDyn1–3) and yellow (inhibitors). Hydrogen bonds are shown as yellow dotted lines with atom distances in Å.

moiety would afford better alignment of the Asp208 –CO₂H to better hydrogen bond with **29**'s 4-CH₂OH. A significant improvement in potency was observed, with **29** displaying an IC₅₀ value of 4.58 ± 0.06 μM, as predicted from our homology model. The positional preference for substituents at the 4-position of the aniline moiety is apparent with the CH₂OH analogues, with the 2-CH₂OH (**27**) inactive and 3-CH₂OH (**28**) significantly less active with an IC₅₀ value of 111 μM. The observed activity increase, by modeling analysis, is a result of the engagement of Ser238's –OH moiety by **29**. Pthaladyn **29**'s –OH group is also predicted to form two additional hydrogen bonds within the binding site where the Asn236 backbone carbonyl acts as a hydrogen bond acceptor and the Ser238 –OH acts as a hydrogen bond donor. Additional van der Waals contacts are also observed between the Val235 side chain and **29**'s CH₂ group (Figure 6C).

The ability to accommodate bulkier groups in close proximity to Asp208 is also evident, with essentially no reduction in dynamin inhibition with the 4-CH₂CO₂H (**31**) and 4-CH₂CH₂CO₂H (**32**) analogues with IC₅₀ values of 95.5 ± 17.5 μM and 104 μM, respectively. In this instance, **32**'s predicted binding pose is similar to that observed with **26** and **28** with efficient engagement of the additional hydrogen bonds associated with Ser238 and Asn236 (not shown). In contrast, the introduction of a 4-CO₂Et moiety removes all activity with **30**, presumably a consequence of additional steric bulk.

Validation of the homology model by examination of the analogues predicted to be active should be strongly supported by the bioevaluation of analogues predicted to have reduced activity. Therefore, within *Library C*, we sought to explore the effect of modifications that increased the steric bulk of the pendent aromatic group. Given our findings relating to steric bulk and the ability of the Asp208 residue to rotate to accommodate bulkier groups and the potential favorable van der Waals contacts with Val235, we synthesized *Library C* in which

Table 4. Inhibition of Dynamin I GTPase Activity by Pthaladyns 34–42

Library C

No	R	IC ₅₀ (μM)
34		112 ± 3.4
35		– ^a
36		– ^a
37		– ^a
38		– ^a
39		– ^a
40		– ^a
41		– ^a
42		84.0 ± 8.5

^a No activity observed at 400 μM.

polar groups were removed and replaced by hydrophobic groups or moved distal to the imide moiety. Synthesis of these analogues was conducted as per Scheme 2 and afforded analogues 34–42 (Table 4). The caveat in this series is that for true engagement of Asp208, the introduction of a polar moiety is required. Thus, our modeling predicted that the introduction of bulky groups would reduce dynamin inhibition, but the combination of bulk and a polar moiety would restore dynamin inhibition. With the exception of the 4-*tert*-butyl substituted 34 (IC₅₀ 112 ± 3.4 μM), all simple aromatic substituted pthaladyns were inactive (35–40). The retention of activity with 34 is a consequence of predicted engagement with Val235 offsetting the reduction in interaction with Asp208, but this latter residue twists to accommodate the bulky 4-*tert*-butyl moiety (not shown). The ability to accommodate changes in hydrophobic bulk is limited, with the simple methylene insertion with the synthesis of 41 rendering this 4-OCH₃ analogue inactive (cf. 21; IC₅₀ 78 ± 10.0 μM). In keeping with our modeling analysis thus far, docking predicted that the introduction of a methyl-2-pyridyl moiety would return the resultant pthaladyn (42) to a modest level

of dynamin inhibition. Synthesis and subsequent screening showed 42 to be an 84 ± 8.5 μM dynamin inhibitor.

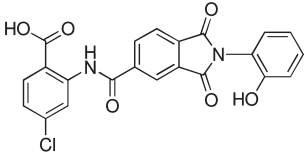
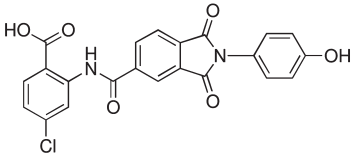
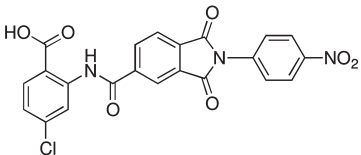
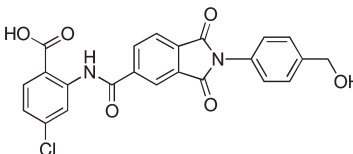
These outcomes strongly suggest that our homology model is valid and is a useful tool for the synthesis of more potent dynamin inhibitors.

Given that dynamin GTPase activity is essential for endocytosis, we next determined the ability of four of our most potent pthaladyns 17, 19, 23, and 29 to block in-cell endocytosis. We first used our well established automated quantitative RME assay based on endocytosis of Texas Red-Tf (Tf-TxR) into U2OS human osteosarcoma cells.^{6,7} After a 30 min preincubation in the presence of increasing concentrations of pthaladyns, 17, 19, 23, and 29, RME was unaffected (Table 5). This was surprising and is the first such incidence where we have noted that all the dynamin active analogues evaluated for RME block were inactive. With the dynoles⁶ and iminodyns,⁷ we noted a considerable, compound dependent, degree of RME block. It is conceivable that the pthaladyns fail to gain entry to the cell, are rapidly degraded or effluxed, or that they are displaying an exquisite degree of dynamin I specificity relative to dynamin II. RME is a dynamin II mediated process, and a lack of RME block may be an indication of dynamin I versus dynamin II specificity. We therefore examined the effect of pthaladyns 17, 19, 23, and 29 directly on the inhibition of dynamin II GTPase activity. While dynamin I in this study was the endogenous form purified from sheep brain, dynamin II was produced as a recombinant protein expressed in Sf9 insect cells. Our dynamin I and dynamin II assays require different dynamin and lipid concentrations to ensure an appropriate optical response in the malachite green assays. This means that we consider the data presented in Table 5 as indicative of specificity only, not as an absolute determination of dynamin I or dynamin II specificity. Notwithstanding this caveat, we obtained dynamin II IC₅₀ curves for pthaladyns 17, 19, 23, and 29 (Table 5). Pthaladyn 17 returned a dynamin II IC₅₀ value of 71.0 μM, essentially indistinguishable from its dynamin I IC₅₀ value. The other pthaladyns displayed varying levels of dynamin I selectivity ranging from 3-fold (19 and 23 with dynamin II IC₅₀ values of 114 and 63.1 μM, respectively) to 9-fold dynamin I selective (29 with dynamin II IC₅₀ value of 40.0 μM), suggesting that these compounds should be considered as pan inhibitors of dynamin (i.e., inhibitors of both dynamin I and II). These data also suggest that the lack of observed RME block is not a consequence of dynamin isoform specificity but more likely is a result of poor cellular uptake or rapid efflux in U2OS cells.

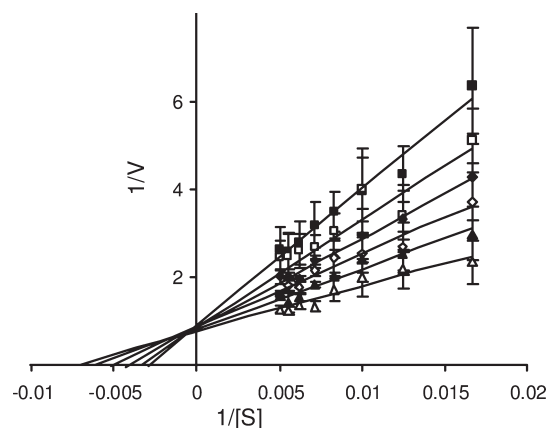
We next determined the effect of pthaladyns 17, 19, 23, and 29 on SVE. This is a dynamin I mediated process in neurons because the concentration of dynamin I in neurons is approximately 50-fold higher than that of dynamin II.⁵³ These studies were conducted using isolated rat brain nerve terminals (synaptosomes), and the effects of the pthaladyns were determined by measuring a change in the uptake of the styryl dye FM4-64, a well characterized endocytic marker in this system.⁵⁴ Only pthaladyn 23 displayed noteworthy inhibition of SVE, returning an IC₅₀ value of 12.9 ± 5.9 μM. The other pthaladyns values were > 100 μM. While pthaladyn-23 had no activity for RME (Table 5), it is a highly effective SVE blocker, acting at close to its dynamin I IC₅₀ (dynamin I IC₅₀ 17.4 ± 5.8 and IC_{50(SVE)} 12.9 ± 5.9 μM). This analogue is therefore a highly efficient inhibitor of SVE.

Finally, to explore the mechanism of inhibition of the pthaladyns on dynamin I, we conducted a series of Michaelis–Menten kinetic experiments with pthaladyn-23 (14–19 μM)

Table 5. Inhibition of Dynamin I or Dynamin II in Vitro GTPase Activity, and in-Cell Receptor Mediated Endocytosis (RME) or Synaptic Vesicle Endocytosis (SVE) by Pthaladyns **17**, **19**, **23**, and **29**

Pthaladyn Compound	Pthaladyn Structure	Dyn I GTPase activity IC ₅₀ (μM) ^a	Dyn II GTPase activity IC ₅₀ (μM) ^b	RME (Tf uptake in U2OS cells) IC ₅₀ (μM) ^b	SVE (FM4-64 uptake in synaptosomes) IC ₅₀ (μM) ^b
17		61 ± 30.0	71 ± 102	NA ^c	119
19		40 ± 10.0	114 ± 30	NA	NA
23		17.4 ± 5.8	63 ± 33	NA	12.9 ± 5.9
29		4.58 ± 0.06	40 ± 49	NA	~690

^aIC₅₀ determinations are the average of at least two independent experiments, each in triplicate. ^bMean ± 95% confidence interval (CI) of a single experiment performed in triplicate. ^cNot active.

**Figure 7.** Competitive kinetics of pthaladyn-**23** with respect to Mg²⁺·GTP. The data depicts pthaladyn-**23** concentration dependent changes in double-reciprocal plot between substrate (GTP at 60–200 μM) and reaction velocity (*V*). The data corresponds to pthaladyn-**23** concentrations of 19 (■) 18 (□), 17 (◆), 16 (◇), 15 (▲), and 14 (Δ) μM. Error bars represent mean ± SEM of four independent experiments each conducted in triplicate.

and varying concentrations of the Mg²⁺·GTP substrate (60–200 μM). The Lineweaver–Burke plots revealed clear competitive inhibition with respect to Mg²⁺·GTP for dynamin

I (Figure 7). This finding confirms that the pthaladyns target the active site, as predicted by the homology model, and they are therefore the first reported active site directed dynamin inhibitors.

Conclusions

Utilizing the high resolution X-ray of the dynamin A GTPase domain, we constructed a number of homology models for the human dynamin I GTPase domain. Two of our modeled structures (hDyn1–3 and hDyn1–7) were able to accommodate GDP in a near native pose and were also consistent with the recently solved X-ray structure of the rat dynamin I GTPase domain. While this work was under review, the crystal structure of human dynamin's GTPase domain was reported.⁵⁵ This is the first report of an active and nucleotide-bound form of dynamin I. The structure within the nucleotide binding pocket was highly similar to our homology model (see Supporting Information). Our homology model was used to screen approximately 800000 compounds in silico to identify potential dynamin I GTPase inhibitors. Pthaladyn-**1** was originally identified as a 170 μM dynamin inhibitor and used as a lead compound in the development of focused compound libraries, including an in-house synthesized version of **1**. Subsequent rescreening showed that **1** was only weakly active against dynamin (IC₅₀ > 400 μM).

Notwithstanding this, our focused and homology modeling-library synthesis has identified the pthaladyns as the first class of GTP competitive inhibitors of dynamin. Two findings strongly demonstrating that our homology models could be used to successfully aid inhibitor design. First, the model guided the development of 4-chloro-2-(2-(4-(hydroxymethyl)-phenyl)-1,3-dioxoisindoline-5-carboxamido)benzoic acid (**29**), a $4.58 \pm 0.06 \mu\text{M}$ potent dynamin inhibitor, a compound approximately 400-fold more potent than the lead. Second, the in-cell active analogue, pthaladyn-**23**, proved to be GTP competitive; the first reported series to compete at the active site of dynamin. Our homology model structures and identified inhibitors are currently being utilized in a number of structure-based drug design projects within our laboratory.

Surprisingly, none of the pthaladyns evaluated (**17**, **19**, **23**, and **29**) blocked RME, which is contrary to our previous findings with the dynoles⁶ and iminodyns,⁷ both of which displayed efficient RME block. This lack of RME block was not an artifact of dynamin I selectivity with, at best, modest levels of dynamin I (versus dynamin II) selectivity being noted. Pthaladyn-**29** displays borderline dynamin I specificity (ca. 9-fold). The lack of RME block is more likely attributed to poor cellular uptake. In a similar vein, only pthaladyn-**23** was an effective inhibitor of dynamin I mediated SVE with an IC_{50} of $12.9 \pm 5.9 \mu\text{M}$ but was an ineffective inhibitor of RME. The basis of its in-cell selectivity is not yet understood.

The vast majority of drugs have one or more off-target actions. In the protein kinase inhibitor field, it has been suggested that a minimum of two structurally unrelated drugs should be used for cell-based studies to minimize such off-target drug actions.⁵⁶ We strongly agree with this principle and suggest that these additional stringent criteria are now available for dynamin. With the advent of the pthaladyns reported here, it is now possible to target dynamin in cell-based studies with up to three chemically unrelated drugs that target three unrelated binding sites in dynamin (GTP binding site: pthaladyns; PH domain: MiTMABs, RTILs; allosteric sites: iminodyns, dynoles, dynasore).^{1–9} The pthaladyns greatly expand the ability to use the dynamin inhibitor palette to more effectively understand dynamins cellular roles. Because of the diversity of cellular systems regulated by the dynamins, these compounds should be evaluated in the future for potential clinical applications in a variety of disorders ranging from cancer to pathogen infection.

Experimental Section

Molecular Modeling Methods. Homology Model Construction. The 2.3 Å crystal structure of the GDP-bound GTPase domain of *Dictyostelium discoideum* dynamin A (PDB code 1JWY) was used as a template to construct a predicted model of the human dynamin I GTPase domain. The homology model was generated using the build model function within ICM 3.1 (Molsoft, San Diego, CA) where the target sequence was aligned on the 3D template (see Supporting Information), missing loops predicted through PDB-database search and the energy of the system minimized by a Monte Carlo simulation through a series of random global moves, and gradient local minimization in the internal coordinates space.⁵⁷

Binding Site Identification. The nucleotide-binding site was defined as an 8 Å sphere surrounding the crystal structure coordinates of dynamin A bound GDP (PDB code 1JWY).

Receptor–Ligand Docking. Initial docking was carried out with a flexible ligand and 0.5 Å grid potential representation of the receptor accounting for hydrophobicity, van der Waals boundaries, hydrogen-bonding profile, and electrostatic potential

of the defined binding site. The resulting conformation was then optimized with flexible ligand and receptor side chains using the refine and dock function within ICM v.3.1.

Virtual Ligand Screening. The ICM virtual library screening function was used to dock ~800000 (Chembridge, San Diego, CA, and Chemical Diversity, San Diego, CA) flexible ligands, which passed a relaxed Lipinski filter (MW < 600, HBA < 12, and HBD < 6) and contained less than seven rotatable bonds onto the receptor grids generated by ICM. Each ligand was assigned a score reflecting the quality of the ligand–receptor complex. Docking was conducted three times in parallel and the lowest score for each ligand was retained. The top ranked 1000 compounds were clustered according to chemical similarity, visually inspected, and compounds displaying significant interactions (1 or more H-bond) with the G2 consensus region were discarded. The top 300 compounds were selected for biological evaluation, of which 175 were still available for purchase.

Biology. Our assay methods for GTPase assay (dynamin I and dynamin II) and in-cell screens (transferrin endocytosis in U2OS cells and FM4–64 uptake in rat brain synaptosomes) have been previously described in detail^{6,7} and are available in the Supporting Information.

Chemistry. General Methods. All solvents were bulk quality and redistilled prior to use. Flash chromatography was carried out using silica gel 200–400 mesh (60 Å). ¹H and ¹³C NMR were recorded at 300 and 75 MHz, respectively, using a Bruker Avance 300 MHz spectrometer in CDCl₃ and DMSO-*d*₆. GCMS was performed using a Shimadzu GCMS-QP2100. The instrument uses a quadrupole mass spectrometer and detects samples via electron impact ionization (EI). The University of Wollongong, Australia, Biomolecular Mass Spectrometry Laboratory analyzed samples for HRMS. The spectra were run on the VG Autospec-oa-tof tandem high resolution mass spectrometer using CI (chemical ionization), with methane as the carrier gas and PFK (perfluorokerosene) as the reference. Microanalysis was conducted at the Microanalysis Unit at the Australian National University, Canberra, Australia. Compound purity was confirmed by a combination of LC-MS (HPLC), micro, and/or high resolution mass spectrometry and NMR analysis. All analogues are ≥95% purity.

General Synthetic Method, Synthesis of 2-Biphenyl-2-yl-1,3-dioxo-2,3-dihydro-1H-isoindole-5-carboxylic Acid Phenylamide (9). To a chilled (0 °C) solution of trimellitic anhydride chloride (0.50 g, 2.4 mmol) in THF (20 mL) was added dropwise a solution of aniline (0.196 g, 2.1 mmol) in 10 mL of the same solvent. The reaction mixture was stirred at 0 °C for 3 h and diluted with EtOAc (30 mL) and 1 M HCl (10 mL). The organic layer was separated, washed with brine (2 × 20 mL), and dried (MgSO₄). The solvent was removed in vacuo to afford crude 1,3-dioxo-*N*-phenyl-1,3-dihydroisobenzofuran-5-carboxamide (**4**), which was used without purification in the next step.

To a suspension of crude **4** (0.128 g, 0.48 mmol) and biphenyl-2-ylamine (0.097 g, 0.56 mmol) in dry toluene (5 mL) was added DMF (1 mL) and triethylamine (0.5 mL). The resulting solution was heated at 130 °C for 18 h, cooled, and partitioned between EtOAc (30 mL) and 1 M HCl (10 mL). The organic layer was separated, washed with brine (2 × 20 mL), dried (MgSO₄), and the solvent removed in vacuo. The residue was purified by flash column chromatography eluting with petrol/EtOAc (8:2), followed by EtOAc to yield the desired compound as a tan solid and then recrystallized from MeOH; Yield 54%; mp 264–265 °C.

¹H NMR (DMSO-*d*₆): δ 7.15 (t, *J* = 7.3 Hz, 1H), 7.26 (m, 5H), 7.34 (m, 2H), 7.55 (m, 4H), 7.76 (d, 7.4 Hz, 2H), 7.99 (d, *J* = 8.1 Hz, 1H), 8.35 (dd, *J* = 1.5, 8.0 Hz, 1H), 8.39 (d, *J* = 1.4 Hz, 1H), 10.51 (s, 1H).

¹³C NMR (DMSO-*d*₆): δ 120.4, 122.2, 123.6, 124.1, 127.5, 127.6, 128.3, 128.4, 128.6, 129.2, 129.7, 130.0, 130.3, 131.4, 133.3, 134.4, 138.2, 138.6, 140.5, 140.9, 163.5, 166.4, 166.5.

2-[(2-Biphenyl-2-yl-1,3-dioxo-2,3-dihydro-1H-isoindole-5-carbonyl)-amino]-4-chlorobenzoic Acid (1). Compound **1** was prepared in a similar manner to the synthesis of **9** from 2-chloro-2-aminobenzoic

acid. The residue was purified by flash column chromatography eluting with petrol/EtOAc (8:2) followed by EtOAc and then recrystallized from MeOH to give a tan solid in a 41% yield (two steps); mp 262–264 °C.

¹H NMR (DMSO-*d*₆): δ 7.01 (dd, *J* = 2.0, 8.3 Hz, 1H), 7.18 (m, 5H), 7.49 (m, 4H), 7.90 (d, *J* = 7.9 Hz, 1H), 8.05 (d, *J* = 8.3 Hz, 1H), 8.32 (s, 1H), 8.41 (d, *J* = 7.8 Hz, 1H), 8.71 (d, *J* = 2.1 Hz, 1H), 15.10 (s, 1H).

¹³C NMR (DMSO-*d*₆): δ 118.3, 121.4, 121.6, 121.9, 123.6, 127.3, 127.5, 128.0, 128.1, 129.1, 129.4, 129.5, 130.3, 131.6, 132.6, 133.3, 133.6, 135.7, 138.1, 140.5, 140.9, 141.4, 162.3, 166.0, 166.1, 170.1.

C₂₈H₁₇ClN₂O₅·0.5H₂O: Calcd C 65.31, H 3.72 N 5.44. Anal. C 65.25, H 3.77, N 5.19.

2-Biphenyl-2-yl-1,3-dioxo-2,3-dihydro-1*H*-isoindole-5-carboxylic Acid (3-Chlorophenyl)amide (10). Compound **10** was prepared in a similar manner to the synthesis of **9** from 3-chloroaniline. The residue was purified by flash column chromatography eluting with petrol/EtOAc (8:2) followed by EtOAc and then recrystallized from MeOH to give a tan solid in a 70% yield (two steps); mp 74–76 °C.

¹H NMR (DMSO-*d*₆): δ 7.16 (m, 7H), 7.40 (m, 4H), 7.62 (s, 1H), 7.80 (d, *J* = 7.4 Hz, 1H), 8.24 (m, 2H), 8.76 (s, 1H) 13.1 (s, 1H).

¹³C NMR (DMSO-*d*₆): δ 118.1, 120.2, 121.4, 123.5, 124.5, 127.0, 127.4, 127.8, 128.0, 128.2, 128.5, 129.3, 129.4, 130.4, 131.3, 133.3, 133.8, 134.0, 137.9, 138.1, 139.7, 140.8, 163.2, 165.9, 166.4.

C₂₇H₁₇ClN₂O₃·3H₂O: Calcd C 63.97, H 4.57 N 5.53. Anal. C 64.00, H 3.71, N 5.47.

2-[(2-Biphenyl-2-yl-1,3-dioxo-2,3-dihydro-1*H*-isoindole-5-carbonyl)amino] Benzoic Acid (11). Compound **11** was prepared in a similar manner to the synthesis of **9** from 2-amino benzoic acid. The residue was purified by flash column chromatography eluting with petrol/EtOAc (8:2) followed by EtOAc and then recrystallized from MeOH to give a tan solid in a 40% yield (two steps); mp 251–53 °C.

¹H NMR (DMSO-*d*₆): δ 7.22 (m, 6H), 7.56 (m, 5H), 8.05 (d, *J* = 7.8 Hz, 2H), 8.31 (s, 1H), 8.37 (dd, *J* = 1.5, 7.8, 1H), 8.59 (d, *J* = 8.3 Hz, 1H), 12.5 (s, 1H).

¹³C NMR (DMSO-*d*₆): δ 119.8, 120.1, 121.4, 123.1, 124.1, 127.5, 127.6, 128.3, 128.4, 129.2, 129.7, 129.8, 130.3, 131.1, 131.8, 132.8, 133.5, 133.7, 138.1, 140.3, 140.5, 140.9, 162.5, 166.2, 166.3, 169.9.

C₂₈H₁₈N₂O₅·2.25H₂O: Calcd C 66.86, H 4.51, N 5.57. Anal. C 66.57, H 4.32, N 5.33.

2-[(2-Biphenyl-2-yl-1,3-dioxo-2,3-dihydro-1*H*-isoindole-5-carbonyl)-amino]-5-iodo Benzoic Acid (12). Compound **12** was prepared in a similar manner to the synthesis of **9** from 5-iodo-2-amino benzoic acid. The residue was purified by flash column chromatography eluting with petrol/EtOAc (8:2) followed by EtOAc and then recrystallized from MeOH to give a tan solid, yield 55% (two steps); mp > 300 °C.

¹H NMR (DMSO-*d*₆): δ 7.26 (m, 5H), 7.56 (m, 4H), 7.97 (dd, *J* = 1.7, 8.6 Hz, 1H), 8.03 (d, *J* = 7.5 Hz, 1H), 8.28 (m, 2H), 8.37 (m, 2H), 12.1 (s, 1H).

¹³C NMR (DMSO-*d*₆): δ 87.0, 120.1, 121.3, 122.7, 124.1, 127.5, 127.6, 128.3, 128.4, 129.2, 129.7, 129.8, 130.1, 130.3, 131.8, 133.7, 138.1, 138.8, 139.7, 139.9, 140.9, 142.2, 162.8, 166.2, 166.3, 168.4.

C₂₈H₁₇I N₂O₅: Calcd C 57.16, H 2.91, N 4.76. Anal. C 57.12, H 2.99, N 4.73.

Synthesis of N-Substituted Pthaladyns 13–42. **4-Chloro-2-[(1,3-dioxo-2-phenyl-2,3-dihydro-1*H*-isoindole-5-carbonyl)amino]-benzoic Acid (13).** To a suspension of **7** (0.15 g, 0.43 mmol) and aniline (0.078 g, 0.65 mmol) in toluene (5 mL) was added DMF (1 mL) and TEA (0.5 mL). The resulting solution was heated at 130 °C for 18 h, cooled, and neutralized with 10% HCl. The solution was partitioned between EtOAc (30 mL) and water (10 mL) and the organic layer separated, washed with brine (2 × 20 mL), dried (MgSO₄), and the solvent removed in vacuo. The residue was purified by flash column chromatography eluting with EtOAc

followed by EtOAc/MeOH (8:2) to yield the desired compound as a brown solid; yield 68%; mp 299–300 °C.

¹H NMR (DMSO-*d*₆): δ 7.26 (dd, *J* = 1.8, 8.4 Hz, 1H), 7.47 (m, 3H), 7.53 (m, 2H), 8.01 (d, *J* = 8.4 Hz, 1H), 8.10 (d, *J* = 7.8 Hz, 1H), 8.30 (s, 1H), 8.35 (d, *J* = 7.8 Hz, 1H), 8.67 (d, *J* = 2.0 Hz, 1H), 12.41 (s, 1H).

¹³C NMR (DMSO-*d*₆): δ 115.8, 119.4, 121.1, 123.3, 124.0, 127.1, 128.1, 128.8, 131.7, 132.1, 132.7, 133.6, 134.2, 138.6, 139.3, 141.4, 162.9, 166.0, 169.3.

C₂₂H₁₃ClN₂O₅·H₂O: Calcd C 60.22, H 3.45, N 6.38. Anal. C 60.41, H 3.46, N 6.51.

2-[(2-(2-Aminophenyl)-1,3-dioxo-2,3-dihydro-1*H*-isoindole-5-carbonyl)amino]-4-chlorobenzoic Acid (14). Synthesized using the general procedure as for **13** with benzene-1,2-diamine to yield the desired compound as a brown solid. Purified by recrystallization from MeOH in a 49% yield; mp > 300 °C.

¹H NMR (DMSO-*d*₆): δ 6.56 (t, *J* = 7.6 Hz, 1H), 6.77 (d, *J* = 7.9 Hz, 1H), 7.01 (dd, *J* = 1.3, 7.8 Hz, 1H), 7.12 (m, 2H), 8.05 (d, *J* = 7.7 Hz, 1H), 8.08 (d, *J* = 8.3 Hz, 1H), 8.40 (s, 1H), 8.45 (d, *J* = 7.8 Hz, 1H), 8.74 (d, *J* = 2.1 Hz, 1H), 12.12 (s, 1H).

¹³C NMR (DMSO-*d*₆): δ 115.2, 115.3, 115.7, 117.9, 121.0, 121.8, 123.4, 123.5, 129.7, 129.8, 132.8, 133.0, 133.1, 134.5, 134.8, 140.0, 141.7, 146.3, 162.8, 166.7, 166.8, 168.7.

C₂₂H₁₄ClN₃O₅·3H₂O: Calcd C 53.94, H 4.12 N 8.58. Anal. C 53.54, H 3.79, N 8.41.

2-[(2-(3-Aminophenyl)-1,3-dioxo-2,3-dihydro-1*H*-isoindole-5-carbonyl)amino]-4-chlorobenzoic Acid (15). Synthesized using the general procedure as for **13** with benzene-1,3-diamine; yield 57%; mp > 300 °C.

¹H NMR (DMSO-*d*₆): δ 6.55 (m, 3H), 7.08 (m, 2H), 8.06 (m, 2H), 8.40 (s, 1H), 8.46 (d, *J* = 7.8 Hz, 1H), 8.72 (d, *J* = 1.8 Hz, 1H), 12.04 (s, 1H).

¹³C NMR (DMSO-*d*₆): δ 112.5, 113.6, 114.4, 117.9, 121.3, 121.9, 123.3, 123.7, 128.9, 132.1, 132.3, 132.8, 133.4, 133.8, 134.5, 140.4, 141.6, 149.2, 162.5, 166.2, 166.3, 168.8.

C₂₂H₁₄ClN₃O₅·4H₂O: Calcd C 52.03, H 4.37, N 8.27. Anal. C 51.98, H 4.72, N 8.24.

2-[(2-(4-Aminophenyl)-1,3-dioxo-2,3-dihydro-1*H*-isoindole-5-carbonyl)amino]-4-chlorobenzoic Acid (16). Synthesized using the general procedure as for **13** with benzene-1,4-diamine; yield 55%; mp > 300 °C.

¹H NMR (DMSO-*d*₆): δ 6.63 (d, *J* = 8.5 Hz, 2H), 7.04 (d, *J* = 8.5 Hz, 2H), 7.11 (dd, *J* = 2.1, 8.4 Hz, 1H), 8.03 (d, *J* = 8.3 Hz, 1H), 8.05 (d, *J* = 7.8 Hz, 1H), 8.37 (s, 1H), 8.42 (d, *J* = 7.8 Hz, 1H), 8.71 (d, *J* = 2.1 Hz, 1H), 12.70 (s, 1H).

¹³C NMR (DMSO-*d*₆): δ 113.4, 118.1, 119.4, 121.2, 122.0, 122.6, 123.6, 128.0, 132.2, 132.8, 133.4, 134.0, 134.9, 140.2, 141.6, 148.8, 162.7, 166.7, 166.8, 169.0.

C₂₂H₁₄ClN₃O₅·3.5H₂O: Calcd C 52.97, H 4.24, N 8.42. Anal. C 52.98, H 3.79, N 8.30.

4-Chloro-2-[(2-(2-hydroxyphenyl)-1,3-dioxo-2,3-dihydro-1*H*-isoindole-5-carbonyl)amino]benzoic Acid (17). Synthesized using the general procedure as for **13** with 2-hydroxyaniline. Purified by recrystallization from MeOH; yield 73%; mp 290–294 °C.

¹H NMR (DMSO-*d*₆): δ 6.92 (dt, *J* = 1.2, 7.5 Hz, 1H), 7.00 (dd, *J* = 2.1, 8.2 Hz, 1H), 7.29 (m, 3H), 8.04 (d, *J* = 8.3 Hz, 1H), 8.12 (d, *J* = 7.7 Hz, 1H), 8.38 (s, 1H), 8.41 (dd, *J* = 1.5, 7.8 Hz, 1H), 8.73 (d, *J* = 2.1 Hz, 1H), 12.84 (s, 1H).

¹³C NMR (DMSO-*d*₆): δ 116.6, 116.9, 118.6, 119.1, 119.4, 121.1, 123.2, 124.0, 130.1, 130.4, 132.6, 132.8, 133.6, 134.6, 138.1, 139.5, 141.4, 153.9, 163.1, 166.2, 166.3, 169.2.

C₂₂H₁₃ClN₂O₆·0.75H₂O: Calcd C 57.34, H 3.43, N 6.08. Anal. C 57.65, H 3.31, N 6.41.

4-Chloro-2-[(2-(3-hydroxyphenyl)-1,3-dioxo-2,3-dihydro-1*H*-isoindole-5-carbonyl)amino]benzoic Acid (18). Synthesized using the general procedure as for **13** with 3-hydroxyaniline. Purified by recrystallization from MeOH; yield 84%; mp 290–291 °C.

¹H NMR (DMSO-*d*₆): δ 6.87 (m, 3H), 7.28 (m, 2H), 8.04 (d, *J* = 8.4 Hz, 1H), 8.11 (d, *J* = 7.8 Hz, 1H), 8.36 (s, 1H), 8.40 (dd, *J* = 1.2, 7.8 Hz, 1H), 8.70 (d, *J* = 2.1 Hz, 1H), 12.85 (s, 1H).

^{13}C NMR (DMSO- d_6): δ 114.3, 115.2, 116.9, 117.7, 119.4, 121.2, 123.2, 124.0, 129.4, 132.2, 132.6, 132.8, 133.6, 134.3, 138.0, 139.5, 141.4, 157.6, 163.1, 166.0, 166.1, 169.2.

$\text{C}_{22}\text{H}_{13}\text{ClN}_2\text{O}_6 \cdot \text{H}_2\text{O}$: Calcd C 57.74, H 3.34, N 6.09. Anal. C 58.10, H 3.32, N 6.09.

4-Chloro-2-[[2-(4-hydroxyphenyl)-1,3-dioxo-2,3-dihydro-1H-isoindole-5-carbonyl]amino]benzoic Acid (19). Synthesized using the general procedure as for **13** with 4-hydroxyaniline. Purified by recrystallization from MeOH; yield 48%; mp > 300 °C.

^1H NMR (DMSO- d_6): δ 6.88 (d, J = 8.7 Hz, 2H), 7.21 (d, J = 8.8 Hz, 2H), 7.31 (dd, J = 2.1, 8.4 Hz, 1H), 8.04 (d, J = 8.4 Hz, 1H), 8.11 (d, J = 7.7 Hz, 1H), 8.34 (s, 1H), 8.38 (dd, J = 1.2, 7.8 Hz, 1H), 8.70 (d, J = 2.0 Hz, 1H), 12.85 (s, 1H).

^{13}C NMR (DMSO- d_6): δ 115.4, 116.1, 119.6, 121.0, 122.6, 123.4, 123.9, 128.6, 132.3, 132.8, 133.5, 134.4, 138.5, 139.6, 141.4, 157.3, 163.2, 166.4, 166.5, 169.2.

$\text{C}_{22}\text{H}_{13}\text{ClN}_2\text{O}_6 \cdot 2.5\text{H}_2\text{O}$: Calcd C 54.84, H 3.77, N 5.81. Anal. C 54.51, H 3.46, N 5.61.

4-Chloro-2-[[2-(3-methoxy)-1,3-dioxo-2,3-dihydro-1H-isoindole-5-carbonyl]amino]benzoic Acid (20). Synthesized using the general procedure as for **13** with 3-methoxyaniline; yield 35%; mp 242–246 °C.

^1H NMR (DMSO- d_6): δ 4.30 (s, 3H), 6.55 (d, J = 8.82 Hz, 1H), 7.61 (d, J = 8.81 Hz, 1H), 7.71 (dd, J = 7.94, 1.80 Hz, 2H), 7.84 (t, J = 6.49, 6.49 Hz, 1H), 7.94 (dd, J = 9.15, 2.66 Hz, 1H), 8.01 (s, 1H), 8.10 (d, J = 10.05 Hz, 1H), 8.20 (dd, J = 7.97, 0.62 Hz, 1H), 8.26 (s, 1H), 8.58 (d, J = 0.82 Hz, 1H), 10.71 (s, 1H).

^{13}C NMR (DMSO- d_6): δ 55.4, 98.5, 100.5, 102.6, 105.8, 107.9, 111.1, 116.9, 120.6, 122.8, 124.9, 128.4, 130.4, 132.5, 133.9, 140.5, 141.7, 149.8, 149.9, 160.2, 161.0, 166.3, 168.9.

$\text{C}_{23}\text{H}_{15}\text{ClN}_2\text{O}_6$: Calcd C 61.28, H 3.35, N 6.21. Anal. C 61.38, H 3.65, N 6.45.

4-Chloro-2-[[2-(4-methoxyphenyl)-1,3-dioxo-2,3-dihydro-1H-isoindole-5-carbonyl]amino]benzoic Acid (21). Synthesized using the general procedure as for **13** with 4-methoxyaniline; yield 25%; mp > 300 °C.

^1H NMR (DMSO- d_6): δ 3.83 (s, 3H), 7.09 (d, J = 8.91 Hz, 2H), 7.23 (m, 3H), 7.38 (d, J = 8.88, 1H), 8.09 (dd, J = 15.36, 8.12 Hz, 2H), 8.4 (s, 1H), 8.44 (dd, J = 7.80, 1.20 Hz, 1H), 8.74 (d, J = 2.12 Hz, 1H), 9.45 (s, 1H).

^{13}C NMR (DMSO- d_6): δ 55.3, 114.1, 114.5, 115.3, 118.3, 121.2, 121.6, 122.2, 123.8, 124.3, 128.6, 132.2, 132.7, 133.5, 134.0, 135.4, 140.2, 141.5, 159.0, 162.2, 162.7, 166.5, 169.0.

$\text{C}_{23}\text{H}_{15}\text{ClN}_2\text{O}_6 \cdot 2\text{H}_2\text{O}$: Calcd C 56.74, H 3.93, N 5.75. Anal. C 56.91, H 4.16, N 5.91.

4-Chloro-2-[[2-(4-methylsulfanyphenyl)-1,3-dioxo-2,3-dihydro-1H-isoindole-5-carbonyl]amino]benzoic Acid (22). Synthesized using the general procedure as for **13** with 4-methylthioaniline; yield 14%; mp 180–182 °C.

^1H NMR (DMSO- d_6): δ 2.32 (s, 3H), 7.28 (dd, J = 8.52, 2.19 Hz, 2H), 7.4 (s, 1H), 8.03 (d, J = 8.54 Hz, 1H), 8.12 (d, J = 7.76 Hz, 2H), 8.34 (s, 1H), 8.40 (d, J = 1.00 Hz, 1H), 8.69 (d, J = 2.04 Hz, 1H), 12.5 (s, 1H).

^{13}C NMR (DMSO- d_6): δ 14.7, 115.4, 116.0, 119.5, 121.1, 123.2, 123.3, 124.0, 126.0, 127.6, 128.5, 130.4, 132.2, 132.7, 133.6, 134.3, 138.5, 138.6, 139.4, 141.4, 163.0, 168.1, 169.2.

$\text{C}_{23}\text{H}_{15}\text{ClN}_2\text{O}_5\text{S}$: Calcd C 59.17, H 3.24, N 6.00. Anal. C 59.51, H 3.39, N 6.51.

4-Chloro-2-[[2-(3-nitrophenyl)-1,3-dioxo-2,3-dihydro-1H-isoindole-5-carbonyl]amino]benzoic Acid (23). Synthesized using the general procedure as for **13** with 3-nitroaniline. Purified by recrystallization from MeOH; yield 56%; mp > 300 °C.

^1H NMR (DMSO- d_6): δ 7.26 (d, J = 8.2 Hz, 1H), 7.85 (m, 1H), 7.93 (m, 2H), 8.05 (d, J = 9.0 Hz, 1H), 8.21 (d, J = 8.1 Hz, 1H), 8.30 (m, 1H), 8.40 (m, 2H), 8.70 (s, 1H), 12.41 (s, 1H).

^{13}C NMR (DMSO- d_6): δ 116.1, 119.6, 121.4, 121.8, 122.8, 123.4, 124.3, 130.3, 132.2, 132.8, 133.5, 133.8, 134.2, 138.5, 139.7, 141.4, 147.8, 162.2, 163.1, 165.7, 165.8, 169.2.

$\text{C}_{22}\text{H}_{12}\text{ClN}_3\text{O}_7$: Calcd C 56.73, H 2.60, N 9.02. Anal. C 56.75, H 2.40, N 8.75.

4-Chloro-2-[[2-(4-nitrophenyl)-1,3-dioxo-2,3-dihydro-1H-isoindole-5-carbonyl]amino]benzoic Acid (24). Synthesized using the general procedure as for **13** with 4-nitroaniline. Purified by recrystallization from MeOH; yield 47%; mp > 300 °C.

^1H NMR (DMSO- d_6): δ 7.30 (d, J = 7.5 Hz, 1H), 7.82 (m, 2H), 8.05 (d, J = 8.4 Hz, 1H), 8.20 (d, J = 7.5 Hz, 1H), 8.39 (m, 4H), 8.71 (s, 1H), 12.54 (s, 1H).

^{13}C NMR (DMSO- d_6): δ 119.7, 121.4, 123.4, 124.1, 124.3, 125.3, 132.2, 132.8, 133.9, 134.2, 137.5, 138.4, 139.8, 141.4, 146.3, 151.2, 163.1, 165.5, 165.6, 169.2.

$\text{C}_{22}\text{H}_{12}\text{ClN}_3\text{O}_7 \cdot 0.25\text{H}_2\text{O}$: Calcd C 56.18, H 2.68, N 8.93. Anal. C 56.29, H 2.66, N 8.72.

2-[[2-(2-Carboxyphenyl)-1,3-dioxo-2,3-dihydro-1H-isoindole-5-carbonyl]amino]-4-chlorobenzoic Acid (25). Synthesized using the general procedure as for **13** with 2-aminobenzoic acid. Purified by recrystallization from MeOH; yield 60%; mp > 300 °C.

^1H NMR (DMSO- d_6): δ 7.31 (dd, J = 2.1, 8.6 Hz, 1H), 7.56 (dd, J = 1.1, 7.9 Hz, 1H), 7.49 (dt, J = 1.4, 7.6 Hz, 1H), 7.78 (dt, J = 1.6, 7.7 Hz, 1H), 8.06 (m, 2H), 8.16 (d, J = 7.7 Hz, 1H), 8.40 (s, 1H), 8.45 (dd, J = 1.5, 7.8 Hz, 1H), 8.71 (d, J = 2.1 Hz, 1H), 12.40 (s, 1H).

^{13}C NMR (DMSO- d_6): δ 116.2, 119.7, 121.3, 123.4, 125.2, 129.0, 129.4, 130.5, 131.0, 131.2, 132.4, 132.8, 133.0, 133.9, 134.3, 138.5, 139.8, 141.4, 163.1, 165.9, 166.1, 166.2, 169.2.

$\text{C}_{23}\text{H}_{15}\text{ClN}_2\text{O}_7 \cdot 0.25\text{H}_2\text{O}$: Calcd C 58.86, H 2.90, N 5.97. Anal. C 58.90, H 3.12, N 6.32.

2-[[2-(4-Carboxyphenyl)-1,3-dioxo-2,3-dihydro-1H-isoindole-5-carbonyl]amino]-4-chlorobenzoic Acid (26). Synthesized using the general procedure as for **13** with 4-aminobenzoic acid. Purified by recrystallization from MeOH; yield 36%; mp > 300 °C.

^1H NMR (DMSO- d_6): δ 7.27 (dd, J = 2.0, 8.6 Hz, 1H), 7.62 (d, J = 7.2 Hz, 2H), 8.02 (d, J = 8.5 Hz, 1H), 8.08 (d, J = 7.2 Hz, 2H), 8.14 (d, J = 7.7 Hz, 1H), 8.36 (s, 1H), 8.39 (d, J = 7.8 Hz, 1H), 8.68 (d, J = 2.0 Hz, 1H), 12.52 (s, 1H).

^{13}C NMR (DMSO- d_6): δ 116.2, 119.5, 121.3, 123.3, 124.2, 126.8, 129.8, 130.2, 132.2, 132.8, 133.7, 134.2, 135.5, 138.4, 139.6, 141.3, 163.0, 165.7, 165.8, 166.6, 169.2.

$\text{C}_{23}\text{H}_{15}\text{ClN}_2\text{O}_7 \cdot 0.5\text{H}_2\text{O}$: Calcd C 58.30, H 2.98, N 5.91. Anal. C 57.97, H 3.40, N 6.26.

4-Chloro-2-[[2-(2-hydroxymethylphenyl)-1,3-dioxo-2,3-dihydro-1H-isoindole-5-carbonyl]amino]benzoic Acid (27). Synthesized using the general procedure as for **13** with (2-aminophenyl)methanol. Purified by recrystallization from MeOH; yield 22%; mp 251–254 °C.

^1H NMR (DMSO- d_6): δ 4.40 (s, 2H), 7.32 (dd, J = 2.0, 8.2 Hz, 1H), 7.39 (m, 2H), 7.49 (dt, J = 1.8, 7.6 Hz, 1H), 7.58 (d, J = 7.4 Hz, 1H), 8.05 (d, J = 8.2 Hz, 1H), 8.16 (d, J = 7.7 Hz, 1H), 8.40 (s, 1H), 8.41 (d, J = 7.8 Hz, 1H), 8.73 (d, J = 2.1 Hz, 1H), 12.44 (s, 1H).

^{13}C NMR (DMSO- d_6): δ 59.7, 116.3, 119.7, 121.3, 123.4, 124.2, 127.4, 127.7, 129.0, 129.1, 129.2, 132.5, 132.8, 133.7, 134.5, 138.5, 139.6, 140.4, 141.4, 163.2, 166.1, 166.2, 169.2.

$\text{C}_{23}\text{H}_{15}\text{ClN}_2\text{O}_6 \cdot 0.5\text{H}_2\text{O}$: Calcd C 60.07, H 3.51, N 6.09. Anal. C 60.22, H 3.68, N 6.38.

4-Chloro-2-[[2-(3-hydroxymethylphenyl)-1,3-dioxo-2,3-dihydro-1H-isoindole-5-carbonyl]amino]benzoic Acid (28). Synthesized using the general procedure as for **13** with (3-aminophenyl)methanol. Purified by recrystallization from MeOH; yield 47%; mp 279–282 °C.

^1H NMR (DMSO- d_6): δ 4.56 (s, 2H), 7.09 (dd, J = 2.2, 8.3 Hz, 1H), 7.32 (d, J = 7.7 Hz, 1H), 7.41 (m, 2H), 7.49 (d, J = 7.7 Hz, 1H), 8.06 (d, J = 8.4 Hz, 1H), 8.12 (d, J = 7.7 Hz, 1H), 8.43 (s, 1H), 8.48 (dd, J = 1.4, 7.8 Hz, 1H), 8.73 (d, J = 2.1 Hz, 1H), 12.41 (s, 1H).

^{13}C NMR (DMSO- d_6): δ 62.4, 115.9, 119.5, 121.1, 123.3, 124.0, 125.1, 125.5, 126.2, 128.5, 131.5, 132.2, 132.8, 133.6, 134.3, 138.6, 139.3, 141.4, 143.5, 163.0, 166.1, 166.2, 169.3.

$\text{C}_{23}\text{H}_{15}\text{ClN}_2\text{O}_6 \cdot 0.75\text{H}_2\text{O}$: Calcd C 59.49, H 3.58, N 6.03. Anal. C 59.49, H 3.59, N 6.21.

4-Chloro-2-[[2-(4-hydroxymethylphenyl)-1,3-dioxo-2,3-dihydro-1H-isoindole-5-carbonyl]amino]benzoic Acid (29). Synthesized using the general procedure as for **13** with (4-aminophenyl)-methanol. Purified by recrystallization from MeOH; yield 28%; mp 296–298 °C.

¹H NMR (DMSO-*d*₆): δ 4.56 (s, 2H), 7.28 (dd, *J* = 2.2, 8.6 Hz, 1H), 7.39 (d, *J* = 8.5 Hz, 2H), 7.48 (d, *J* = 8.3 Hz, 2H), 8.04 (d, *J* = 8.5 Hz, 1H), 8.13 (d, *J* = 7.7 Hz, 1H), 8.35 (s, 1H), 8.38 (d, *J* = 7.8 Hz, 1H), 8.70 (d, *J* = 2.1 Hz, 1H), 12.41 (s, 1H).

¹³C NMR (DMSO-*d*₆): δ 62.4, 116.0, 119.6, 121.1, 123.4, 124.0, 126.7, 126.9, 130.1, 132.3, 132.8, 133.6, 134.3, 138.5, 139.4, 141.4, 142.7, 163.1, 166.1, 166.2, 169.2.

C₂₃H₁₅ClN₂O₆·0.75H₂O: Calcd C 59.49, H 3.58, N 6.03. Anal. C 59.49, H 3.59, N 6.21.

4-Chloro-2-[[2-(4-ethoxycarbonylphenyl)-1,3-dioxo-2,3-dihydro-1H-isoindole-5-carbonyl]-amino]benzoic Acid (30). Synthesized using the general procedure as for **13** with ethyl 4-aminobenzoate; yield 18%; mp > 300 °C.

¹H NMR (DMSO-*d*₆): δ 1.04 (t, *J* = 7.0, 6.99 Hz, 3H), 2.06 (m, 2H), 6.58 (dd, *J* = 2.6, 9.8 Hz, 2H), 7.83 (d, *J* = 8.0 Hz, 1H), 7.91 (d, *J* = 9.2 Hz, 1H), 8.20 (d, *J* = 8.0 Hz, 1H), 8.46 (dd, *J* = 1.6, 8.0 Hz, 2H), 8.58 (d, *J* = 0.8 Hz, 1H), 11.0 (s, 1H).

¹³C NMR (DMSO-*d*₆): δ 13.7, 61.2, 126.4, 126.9, 129.1, 129.2, 129.4, 129.8, 131.3, 131.7, 133.4, 133.8, 140.5, 140.6, 140.8, 140.9, 166.9, 167.3, 167.4, 167.8.

HRMS: calcd for C₂₅H₁₇ClN₂O₇ 492.0724; found (ESI⁺) (M + H) 492.0724.

2-[[2-(4-Carboxymethylphenyl)-1,3-dioxo-2,3-dihydro-1H-isoindole-5-carbonyl]-amino]-4-chlorobenzoic Acid (31). Synthesized using the general procedure as for **13** with 2-(4-aminophenyl)-acetic acid; yield 43%; mp > 272–275 °C.

¹H NMR (DMSO-*d*₆): δ 3.7 (s, 2H), 7.28 (dd, *J* = 2.1, 8.5 Hz, 2H), 7.40 (m, 2H), 8.02 (d, *J* = 8.5 Hz, 2H), 8.12 (d, *J* = 7.8 Hz, 1H), 8.33 (s, 1H), 8.38 (d, *J* = 7.8 Hz, 2H), 8.68 (d, *J* = 1.9 Hz, 1H), 12.4 (s, 1H).

¹³C NMR (DMSO-*d*₆): δ 45.4, 115.9, 119.5, 121.1, 123.4, 124.0, 127.0, 129.8, 130.1, 132.2, 132.8, 133.6, 134.3, 135.2, 138.6, 139.3, 141.4, 163.0, 166.1, 169.3, 172.3.

HRMS: calcd for C₂₄H₁₅ClN₂O₇ 478.0568; found (ESI⁺) (M + H) 478.0568.

2-[[2-[4-(2-Carboxyethyl)-phenyl]-1,3-dioxo-2,3-dihydro-1H-isoindole-5-carbonyl]-amino]-4-chlorobenzoic Acid (32). Synthesized using the general procedure as for **13** with 3-(4-aminophenyl)propanoic acid; yield 16%; mp > 227–229 °C.

¹H NMR (DMSO-*d*₆): δ 2.81 (m, 4H), 7.13 (d, *J* = 8.2 Hz, 1H), 7.31 (dd, *J* = 1.6, 8.0 Hz, 1H), 7.37 (s, 1H), 7.45 (d, *J* = 8.0 Hz, 1H), 8.05 (d, *J* = 8.0 Hz, 1H), 8.14 (d, *J* = 7.3 Hz, 1H), 8.37 (s, 1H), 8.41 (d, *J* = 7.4 Hz, 1H), 8.72 (d, *J* = 1.5 Hz, 1H), 9.74 (s, 1H), 12.46 (s, 1H).

¹³C NMR (DMSO-*d*₆): δ 34.5, 35.0, 116.3, 119.1, 119.6, 121.2, 123.4, 124.1, 127.1, 128.3, 128.6, 129.7, 132.3, 132.8, 133.7, 134.3, 137.1, 138.4, 139.5, 141.4, 163.1, 166.2, 169.2, 170.1, 172.5.

HRMS: calcd for C₂₅H₁₇ClN₂O₇ 492.0724; found (ESI⁺) (M + H) 492.0725.

2-[[2-(3-Hydroxy-4-carboxyphenyl)-1,3-dioxo-2,3-dihydro-1H-isoindole-5-carbonyl]-amino]-4-chlorobenzoic Acid (33). Synthesized using the general procedure as for **13** with 4-amino-3-hydroxybenzoic acid; yield 7%; mp > 242–244 °C.

¹H NMR (DMSO-*d*₆): δ 6.90 (s, 1H), 7.13 (d, *J* = 8.2 Hz, 1H), 7.30 (m, 2H), 7.81 (d, *J* = 8.1 Hz, 1H), 8.04 (s, 1H), 8.09 (d, *J* = 8.6 Hz, 1H), 8.4 (s, 1H), 8.44 (d, *J* = 7.8 Hz, 1H), 8.74 (d, *J* = 9.7 Hz, 1H), 10.4 (s, 1H).

¹³C NMR (DMSO-*d*₆): δ 114.1, 114.7, 115.2, 117.7, 118.2, 121.3, 122.2, 123.9, 129.4, 130.0, 132.2, 132.6, 132.8, 133.5, 133.9, 135.2, 140.2, 141.5, 157.6, 162.6, 166.2, 169.1, 171.2.

HRMS: calcd for C₂₃H₁₃ClN₂O₈ 480.03604; found (ESI⁺) (M + H) 480.

2-[[2-(4-*tert*-Butylphenyl)-1,3-dioxo-2,3-dihydro-1H-isoindole-5-carbonyl]-amino]-4-chlorobenzoic Acid (34). Synthesized using

the general procedure as for **13** with 4-*tert*-butylaniline; yield 14%; mp > 300 °C.

¹H NMR (DMSO-*d*₆): δ 1.26 (m, 9H), 6.50 (d, *J* = 8.5 Hz, 1H), 7.02 (d, *J* = 8.5 Hz, 1H), 7.20 (d, *J* = 8.4 Hz, 1H), 7.34 (d, *J* = 8.5 Hz, 1H), 7.59 (dd, *J* = 3.5, 8.5 Hz, 2H), 7.72 (d, *J* = 7.9 Hz, 1H), 8.06 (m, 1H), 8.17 (dd, *J* = 1.9, 8.0 Hz, 1H), 8.77 (dd, *J* = 2.0, 7.2 Hz, 1H), 10.34 (s, 1H).

¹³C NMR (DMSO-*d*₆): δ 31.4, 33.9, 113.9, 118.7, 119.3, 122.5, 125.3, 126.4, 126.8, 127.8, 128.2, 128.5, 130.1, 130.6, 132.8, 135.0, 136.7, 139.1, 141.8, 145.4, 145.8, 163.4, 166.3, 166.9, 169.2.

HRMS: calcd for C₂₆H₂₁ClN₂O₅ 476.1139; found (ESI⁺) (M + H) 476.1140.

4-Chloro-2-[[2-(2,6-dimethylphenyl)-1,3-dioxo-2,3-dihydro-1H-isoindole-5-carbonyl]-amino]benzoic Acid (35). Synthesized using the general procedure as for **13** with 2,6-dimethylaniline; yield 47%; mp 224–226 °C.

¹H NMR (DMSO-*d*₆): δ 2.17 (s, 6H), 6.63 (t, *J* = 7.5 Hz, 1H), 6.93 (d, *J* = 7.5 Hz, 1H), 7.04 (d, *J* = 2.0 Hz, 1H), 7.07 (m, 2H), 7.20 (d, *J* = 7.4 Hz, 1H), 8.08 (d, *J* = 7.7 Hz, 1H), 8.13 (dd, *J* = 3.4, 8.4 Hz, 1H), 8.24 (dd, *J* = 1.7, 8.2 Hz, 1H), 8.40 (d, *J* = 8.2 Hz, 1H), 8.62 (s, 1H), 9.0 (s, 1H).

¹³C NMR (DMSO-*d*₆): δ 12.6, 20.7, 113.4, 117.3, 118.8, 119.2, 120.8, 123.7, 124.9, 128.3, 129.0, 130.3, 131.4, 133.2, 134.6, 138.0, 139.3, 140.1, 142.8, 145.6, 161.2, 163.4, 165.8, 166.0.

HRMS: calcd for C₂₄H₁₇ClN₂O₅ 448.0826; found (ESI⁺) (M + H) 448.0829.

4-Chloro-2-[[2-(1-naphthalen-1-yl)-1,3-dioxo-2,3-dihydro-1H-isoindole-5-carbonyl]-amino]benzoic Acid (36). Synthesized using the general procedure as for **13** with 1-naphthylamine; yield 7%; mp > 300 °C.

¹H NMR (DMSO-*d*₆): δ 6.84 (s, 1H), 6.93 (d, *J* = 8.0 Hz, 1H), 7.07 (m, 2H), 7.26 (d, *J* = 7.0 Hz, 1H), 7.48 (d, *J* = 7.7 Hz, 1H), 7.6 (m, 2H), 7.82 (d, *J* = 7.7 Hz, 1H), 8.03 (d, *J* = 6.3 Hz, 1H), 8.15 (d, *J* = 7.3 Hz, 1H), 8.38 (m, 2H), 8.73 (s, 1H), 12.45 (s, 1H).

¹³C NMR (DMSO-*d*₆): δ 106.3, 116.2, 118.4, 119.5, 120.9, 121.2, 123.1, 124.1, 125.9, 127.5, 128.9, 130.2, 132.8, 133.7, 134.9, 135.9, 136.2, 138.5, 139.5, 141.6, 145.9, 163.1, 168.2, 167.5, 169.4.

HRMS: calcd for C₂₆H₁₅ClN₂O₅ 470.0670; found (ESI⁺) (M + H) 470.0667.

4-Chloro-2-[[1,3-dioxo-2-(1,2,3,4-tetrahydronaphthalen-1-yl)-2,3-dihydro-1H-isoindole-5-carbonyl]-amino]benzoic Acid (37). Synthesized using the general procedure as for **13** with 1-amino-1,2,3,4-tetrahydronaphthalene; yield 11%; mp > 256–258 °C.

¹H NMR (DMSO-*d*₆): δ 1.9 (m, 6H), 4.45 (t, *J* = 5.2 Hz, 1H), 7.19 (m, 4H), 7.47 (d, *J* = 7.7 Hz, 1H), 8.07 (dd, *J* = 8.5 Hz, 2H), 8.16 (d, *J* = 8.2 Hz, 1H), 8.36 (m, 2H), 8.66 (d, *J* = 1.2 Hz, 1H), 8.77 (d, *J* = 2.0 Hz, 1H), 10.3 (s, 1H).

¹³C NMR (DMSO-*d*₆): δ 18.1, 27.4, 28.3, 47.9, 118.6, 118.7, 122.5, 122.6, 126.0, 128.1, 128.4, 128.9, 129.2, 130.2, 131.8, 132.4, 132.8, 134.6, 135.7, 136.9, 137.5, 141.8, 163.7, 167.3, 167.4, 169.3.

HRMS: calcd for C₂₆H₁₉ClN₂O₅ 474.0983; found (ESI⁺) (M + H) 474.0984.

2-[[2-(Benzyl-1,3-dioxo-2,3-dihydro-1H-isoindole-5-carbonyl)-amino]-4-chloro-benzoic Acid (38). Synthesized using the general procedure as for **13** with benzylamine; yield 25%; mp 236–238 °C.

¹H NMR (DMSO-*d*₆): δ 4.80 (s, 2H), 7.08 (dd, *J* = 2.1, 8.3 Hz, 2H), 7.2 (m, 3H), 8.05 (d, *J* = 8.8 Hz, 1H), 8.35 (m, 3H), 8.42 (s, 1H), 8.56 (d, *J* = 7.5 Hz, 1H), 12.42 (s, 1H).

¹³C NMR (DMSO-*d*₆): δ 45.8, 113.5, 117.8, 119.4, 120.7, 124.4, 125.2, 128.8, 129.5, 130.3, 131.2, 132.9, 133.6, 135.8, 137.3, 138.9, 141.5, 145.6, 150.0, 162.1, 165.5, 165.6, 167.8.

HRMS: calcd for C₂₃H₁₅ClN₂O₈ 434.0670; found (ESI⁺) (M + H) 434.0671.

4-Chloro-2-[[1,3-dioxo-2-(2-phenethyl)-2,3-dihydro-1H-isoindole-5-carbonyl]-amino]benzoic Acid (39). Synthesized using the general procedure as for **13** with 2-phenylethanamine; yield 16%; mp 274–277 °C.

¹H NMR (DMSO-*d*₆): δ 5.13 (m, 4H), 7.25 (m, 5H), 7.41 (d, *J* = 7.0 Hz, 1H), 7.59 (d, *J* = 7.9 Hz, 1H), 8.03 (dd, *J* = 3.0, 5.5 Hz, 1H), 8.11 (dd, *J* = 1.7, 7.9 Hz, 1H), 8.26 (s, 1H), 8.37 (d, *J* = 1.5 Hz, 1H), 8.75 (d, *J* = 2.0 Hz, 1H), 12.46 (s, 1H).

¹³C NMR (DMSO-*d*₆): δ 42.0, 48.2, 115.7, 119.4, 121.0, 123.0, 126.1, 126.5, 127.8, 128.1, 128.7, 130.0, 130.8, 132.8, 133.4, 134.3, 138.5, 141.8, 142.1, 144.2, 163.1, 163.5, 166.9, 169.4.

HRMS: calcd for C₂₄H₁₇ClN₂O₅ 448.0826; found (ESI⁺) (M + H) 448.0827.

4-Chloro-2-[[1,3-dioxo-2-(4-phenylbutyl)-2,3-dihydro-1H-isoindole-5-carbonyl]-amino]benzoic Acid (40). Synthesized using the general procedure as for **13** with 4-phenylbutanamine; yield 21%; mp 214–216 °C.

¹H NMR (DMSO-*d*₆): δ 1.15 (t, *J* = 7.1 Hz, 4H), 1.96 (d, *J* = 2.3 Hz, 2H), 2.5 (m, 2H), 3.59 (d, *J* = 6.1 Hz, 2H), 7.2 (m, 5H), 8.00 (dd, *J* = 5.5, 8.1 Hz, 1H), 8.22 (s, 1H), 8.28 (d, *J* = 1.3 Hz, 1H), 8.31 (d, *J* = 1.3 Hz, 1H), 8.66 (d, *J* = 2.1 Hz, 1H), 11.63 (s, 1H).

¹³C NMR (DMSO-*d*₆): δ 27.4, 28.2, 34.5, 37.4, 116.3, 119.4, 120.8, 123.2, 123.6, 125.6, 128.2, 132.3, 132.8, 133.2, 134.3, 138.3, 139.1, 141.4, 141.8, 162.9, 166.9, 169.1, 169.2.

HRMS: calcd for C₂₆H₂₁ClN₂O₅ 476.1139; found (ESI⁺) (M + H) 476.1141.

4-Chloro-2-[[2-(4-methoxybenzyl)-1,3-dioxo-2,3-dihydro-1H-isoindole-5-carbonyl]-amino]benzoic Acid (41). Synthesized using the general procedure as for **13** with 4-methoxybenzyl amine; yield 14%; mp 250–252 °C.

¹H NMR (DMSO-*d*₆): δ 3.98 (s, 3H), 4.71 (s, 2H), 6.86 (d, *J* = 8.7 Hz, 2H), 6.93 (d, *J* = 8.7 Hz, 2H), 7.14 (d, *J* = 2.2 Hz, 1H), 7.25 (d, *J* = 8.7 Hz, 1H), 7.37 (d, *J* = 8.7 Hz, 1H), 8.04 (d, *J* = 8.3 Hz, 1H), 8.33 (s, 1H), 8.37 (dd, *J* = 1.3, 7.8 Hz, 1H), 8.71 (d, *J* = 2.2 Hz, 1H), 11.64 (s, 1H).

¹³C NMR (DMSO-*d*₆): δ 15.1, 64.8, 106.8, 110.4, 124.6, 125.9, 127.2, 129.1, 129.4, 129.5, 131.3, 132.9, 134.0, 134.7, 135.3, 139.7, 140.5, 145.2, 145.9, 157.6, 162.7, 166.7, 167.1, 168.2.

HRMS: calcd for C₂₄H₁₇ClN₂O₆ 464.0775; found (ESI⁺) (M + H) 464.0777.

4-Chloro-2-[[1,3-dioxo-2-pyridin-3-ylmethyl-2,3-dihydro-1H-isoindole-5-carbonyl]-amino]benzoic Acid (42). Synthesized using the general procedure as for **13** with 3-pyridylmethyl amine; yield 38%; mp > 300 °C.

¹H NMR (DMSO-*d*₆): δ 4.83 (s, 2H), 7.11 (dd, *J* = 2.0, 8.4, 2.02 Hz, 1H), 7.33 (d, *J* = 5.4 Hz, 1H), 7.46 (d, *J* = 5.4 Hz, 1H), 8.05 (dd, *J* = 3.7, 8.0 Hz, 1H), 8.38 (s, 1H), 8.42 (d, *J* = 7.8 Hz, 1H), 8.50 (d, *J* = 5.5 Hz, 1H), 8.57 (d, *J* = 5.5 Hz, 1H), 8.72 (d, *J* = 2.0 Hz, 1H), 8.76 (d, *J* = 1.9 Hz, 1H), 8.82 (d, *J* = 1.4 Hz, 1H), 10.41 (s, 1H).

¹³C NMR (DMSO-*d*₆): δ 41.1, 118.1, 121.3, 122.0, 123.1, 123.8, 128.4, 132.3, 132.7, 133.4, 133.9, 135.9, 137.7, 140.3, 141.5, 142.9, 145.1, 149.7, 162.6, 167.1, 167.6, 169.2.

HRMS: calcd for C₂₂H₁₄ClN₃O₅ 435.0622; found (ESI⁺) (M + H) 435.0624.

Acknowledgment. We are grateful for financial support from the NH & MRC (Australia), the Children's Medical Research Institute (CMRI), and the University of Newcastle (UoN). L.O. and D.H. gratefully acknowledge scholarship support from UN & CMRI and AusAid respectively.

Supporting Information Available: Additional general synthesis information, details of screening methods, sequence alignment, and graphical output from Proflex. This material is available free of charge via the Internet at <http://pubs.acs.org>.

References

- Hill, T. A.; Odell, L. R.; Quan, A.; Abagyan, R.; Ferguson, G.; Robinson, P. J.; McCluskey, A. Long chain amines and long chain ammonium salts as novel inhibitors of dynamin GTPase activity. *Bioorg. Med. Chem. Lett.* **2004**, *14*, 3275–3278.
- Quan, A. M.; McGeachie, A. B.; Keating, D. J.; van Dam, E. M.; Rusak, J.; Chau, N.; Malladi, C. S.; Chen, C.; McCluskey, A.; Cousin, M. A.; Robinson, P. J. Myristyl trimethyl ammonium bromide and octadecyl trimethyl ammonium bromide are surface-active small molecule dynamin inhibitors that block endocytosis mediated by dynamin I or dynamin II. *Mol. Pharmacol.* **2007**, *72*, 1425–1439.
- Hill, T. A.; Odell, L. R.; Edwards, J. K.; Graham, M. E.; McGeachie, A. B.; Rusak, J.; Quan, A.; Abagyan, R.; Scott, J. L.; Robinson, P. J.; McCluskey, A. Small molecule inhibitors of dynamin I GTPase activity: development of dimeric tryphostins. *J. Med. Chem.* **2005**, *48*, 7781–7788.
- Odell, L. R.; Chau, N.; Mariana, A.; Graham, M. E.; Robinson, P. J.; McCluskey, A. Azido and Diaziriny Analogs of Bis-Tryphostin as Asymmetrical Inhibitors of Dynamin GTPase. *ChemMedChem* **2009**, *4*, 1182–1188.
- Zhang, J. L.; Lawrence, G. A.; Chau, N.; Robinson, P. J.; McCluskey, A. From Spanish fly to room-temperature ionic liquids (RTILs): synthesis, thermal stability and inhibition of dynamin I GTPase by a novel class of RTILs. *New J. Chem.* **2008**, *32*, 28–36.
- Hill, T. A.; Gordon, C. P.; McGeachie, A. B.; Venn-Brown, B.; Odell, L. R.; Chau, N.; Quan, A.; Mariana, A.; Sakoff, J. A.; Chircop, M.; Robinson, P. J.; McCluskey, A. Inhibition of dynamin I mediated endocytosis by the dynoles—synthesis and functional activity of a family of indoles. *J. Med. Chem.* **2009**, *52*, 3762–3773.
- Hill, T. A.; Mariana, A.; Gordon, C. P.; Odell, L. R.; Robertson, M. J.; McGeachie, A. B.; Chau, N.; Daniel, J. A.; Gorgani, N. N.; Robinson, P. J.; McCluskey, A. Iminochromene inhibitors of dynamin I & II GTPase activity and endocytosis. *J. Med. Chem.* **2010**, *53*, 4094–4102.
- Macia, E.; Ehrlich, M.; Massol, R.; Boucrot, E.; Brunner, C.; Kirchhausen, T. Dynasore, a cell-permeable inhibitor of dynamin. *Dev. Cell* **2006**, *10*, 839–850.
- Otomo, M.; Takahashi, K.; Miyoshi, H.; Osada, K.; Nakashima, H.; Yamaguchi, N. Some selective serotonin reuptake inhibitors inhibit dynamin I guanosine triphosphatase (GTPase). *Biol. Pharm. Bull.* **2008**, *31*, 1489–1495.
- Brodsky, F. M.; Chen, C. Y.; Knuehl, C.; Towler, M. C.; Wakeham, D. E. Biological basket weaving: formation and function of clathrin-coated vesicles. *Annu. Rev. Cell Dev. Biol.* **2001**, *17*, 517–568.
- Stowell, M. H. B.; Marks, B.; Wigge, P.; McMahon, H. T. Nucleotide-dependent conformational changes in dynamin: evidence for a mechanochemical molecular spring. *Nat. Cell Biol.* **1999**, *1*, 27–32.
- Timm, D.; Salim, K.; Gout, I.; Guruprasad, L.; Waterfield, M.; Blundell, T. Crystal structure of the pleckstrin homology domain from dynamin. *Nat. Struct. Biol.* **1994**, *1*, 782–788.
- Ferguson, K. M.; Lemmon, M. A.; Schlessinger, J.; Sigler, P. B. Crystal structure at 2.2 Å resolution of the pleckstrin homology domain from human dynamin. *Cell* **1994**, *79*, 199–209.
- Downing, A. K.; Driscoll, P. C.; Gout, I.; Salim, K.; Zvebil, M. J.; Waterfield, M. D. Three-dimensional solution structure of the pleckstrin homology domain from dynamin. *Curr. Biol.* **1994**, *4*, 884–891.
- Fushman, D.; Cahill, S.; Lemmon, M. A.; Schlessinger, J.; Cowburn, D. Solution structure of pleckstrin homology domain of dynamin by heteronuclear NMR spectroscopy. *Proc. Natl. Acad. Sci. U.S.A.* **1995**, *92*, 816–820.
- Fushman, D.; Cahill, S.; Cowburn, D. The main-chain dynamics of the dynamin pleckstrin homology (PH) domain in solution: analysis of ¹⁵N relaxation with monomer/dimer equilibration. *J. Mol. Biol.* **1997**, *266*, 173–194.
- Zuchner, S.; Noureddine, M.; Kennerson, M.; Verhoeven, K.; Claeys, K.; Jonghe, P. D.; Merory, J.; Oliveira, S. A.; Speer, M. C.; Zhu, D.; Pericak-Vance, M. A.; Nicholson, G.; Timmerman, V.; Vance, J. M. Mutations in the pleckstrin homology domain of dynamin 2 cause dominant intermediate Charcot-Marie-Tooth disease. *Nat. Genet.* **2005**, *37*, 289–294.
- Bitou, M.; Maugenre, S.; Jeannet, P. -Y.; Lacène, E.; Ferrer, X.; Laforêt, P.; Martin, J. -J.; Laporte, J.; Lochmüller, H.; Beggs, A. H.; Fardeau, M.; Eymard, B.; Romero, N. B.; Guicheney, P. Mutations in dynamin 2 cause dominant centronuclear myopathy. *Nat. Genet.* **2005**, *37*, 1207–1209.
- Salim, K.; Bottomley, M. J.; Querfurth, E.; Zvebil, M. J.; Gout, I.; Scaife, R.; Margolis, R. L.; Gigg, R.; Smith, C. I. E.; Driscoll, P. C.; Waterfield, M. D.; Panayotou, G. Distinct specificity in the recognition of phosphoinositides by the pleckstrin homology domains of dynamin and Bruton's tyrosine kinase. *EMBO J.* **1996**, *15*, 6241–6250.
- Thompson, H. M.; Cao, H.; Chen, J.; Euteneur, U.; McNiven, M. A. Dynamin 2 binds gamma-tubulin and participates in centrosome cohesion. *Nat. Cell Biol.* **2004**, *335*–342.

- (21) Binns, D. D.; Helms, M. K.; Barylko, B.; Davis, C. T.; Jameson, D. M.; Abanesi, J. P.; Eccleston, J. F. The mechanism of GTP hydrolysis by dynamin II: a transient kinetic study. *Biochemistry* **2000**, *39*, 7188–7196.
- (22) Sever, S.; H. Damke, H.; Schmid, S. L. Garrotes, springs, ratchets, and whips: putting dynamin models to the test. *Traffic* **2000**, *5*, 385–392.
- (23) McLure, S. J.; Robinson, P. J. Dynamin, endocytosis and intracellular signaling. *Mol. Memb. Biol.* **1996**, *13*, 189–215.
- (24) Cousin, M. A. R.; Robinson, P. J. Mechanisms of synaptic vesicle recycling illuminated by fluorescent dyes. *J. Neurochem.* **1999**, *73*, 2227–2239.
- (25) Cousin, M. A. R.; Robinson, P. J. The dephosphins: dephosphorylation by calcineurin triggers synaptic vesicle endocytosis. *Trends Neurosci.* **2001**, *24*, 659–665.
- (26) Conner, S. D.; Schmid, S. L. Regulated portals of entry into the cell. *Nature* **2003**, *422*, 37–44.
- (27) Clayton, E. L.; Cousin, M. A. The molecular physiology of activity-dependent bulk endocytosis of synaptic vesicles. *J. Neurochem.* **2009**, *111*, 901–914.
- (28) Doherty, G. J.; McMahon, H. T. Mechanisms of endocytosis. *Annu. Rev. Biochem.* **2009**, *78*, 857–902.
- (29) Mettlen, M.; Stoerber, M.; Loerke, D.; Antonescu, C. N.; Danuser, G.; Schmid, S. L. Endocytic accessory proteins are functionally distinguished by their differential effects on the maturation of clathrin-coated pits. *Mol. Biol. Cell* **2009**, *20*, 3251–3260.
- (30) Rappoport, J. Z. Focusing on clathrin-mediated endocytosis. *Biochem. J.* **2008**, *412*, 415–423.
- (31) Roux, A.; Uyhazi, K.; Frost, A.; De Camilli, P. GTP-dependent twisting of dynamin implicates constriction and tension in membrane fission. *Nature* **2006**, *441*, 528–531.
- (32) Anggono, V.; Smillie, K. J.; Graham, M. E.; Valova, V. A.; Cousin, M. A.; Robinson, P. J. Syndapin I is the phosphorylation-regulated dynamin I partner in synaptic vesicle endocytosis. *Nat. Neurosci.* **2006**, *9*, 752–760.
- (33) Joshi, S.; Gaddipati, S.; Gilbert, J.; Smith, C. M.; Mariana, A.; Gordon, C. P.; Sakoff, J. A.; McCluskey, A.; Robinson, P. J.; Braithwaite, A. W.; Chircop, M. The dynamin inhibitors MiT-MAB and OcTMAB induce cytokinesis failure and inhibit cell proliferation in human cancer cells. *Mol. Cancer Ther.* **2010**, in press.
- (34) Miyauchi, K.; Kim, Y.; Latinovic, O.; Morozov, V.; Melikyan, G. B. HIV enters cells via endocytosis and dynamin-dependent fusion with endosomes. *Cell* **2009**, *137*, 433–444.
- (35) Shoichet, B. K. Virtual screening of chemical libraries. *Nature* **2004**, *432*, 862–865.
- (36) Schneider, G. Virtual screening: an endless staircase? *Nature Rev. Drug Discovery* **2010**, *9*, 273–276 and references cited therein.
- (37) Okamoto, M.; Takayama, K.; Shimizu, T.; Ishida, K.; Takahashi, O.; Furuya, T. Identification of Death-Associated Protein Kinases Inhibitors Using Structure-Based Virtual Screening. *J. Med. Chem.* **2009**, *52*, 7323–7327.
- (38) Herschhorn, A.; Hizi, A. Virtual Screening, Identification, and Biochemical Characterization of Novel Inhibitors of the Reverse Transcriptase of Human Immunodeficiency Virus Type-1. *J. Med. Chem.* **2008**, *51*, 5702–5713.
- (39) Selvam, C.; Oueslati, N.; Lemasson, I. A.; Brabet, A.; Rigault, D.; Courtiol, T.; Cesarini, S.; Triballeau, N.; Bertrand, H. -O.; Goudet, C.; Pin, J. -P.; Acher, F. C. A Virtual Screening Hit Reveals New Possibilities for Developing Group III Metabotropic Glutamate Receptor Agonists. *J. Med. Chem.* **2010**, *53*, 2797–2813.
- (40) Podvinec, M.; Lim, S. P.; Schmidt, T.; Scarsi, M.; Wen, D.; Sonntag, L. -S.; Sanschagrin, P.; Shenkin, P. S.; Schwede, T. Novel Inhibitors of Dengue Virus Methyltransferase: Discovery by In Vitro-Driven Virtual Screening on a Desktop Computer Grid. *J. Med. Chem.* **2010**, *53*, 1483–1495.
- (41) Basse, N.; Montes, M.; Marchal, X.; Qin, L.; Bouvier-Durand, M.; Genin, E.; Vidal, J.; Villoutreix, B. O.; Reboud-Ravaux, M. Novel Organic Proteasome Inhibitors Identified by Virtual and in Vitro Screening. *J. Med. Chem.* **2010**, *53*, 509–513.
- (42) Li, H.; Huang, J.; Chen, L.; Liu, X.; Chen, T.; Zhu, J.; Lu, W.; Shen, X.; Li, J.; Hilgenfeld, R.; Jiang, H. Identification of Novel Falcipain-2 Inhibitors as Potential Antimalarial Agents through Structure-Based Virtual Screening. *J. Med. Chem.* **2009**, *52*, 4936–4940.
- (43) Moulton, J. Predicting protein three-dimensional structure. *Curr. Opin. Biotechnol.* **1999**, *10*, 583–588.
- (44) Bourne, H. R.; Sanders, D. A.; McCormick, F. The GTPase superfamily: conserved structure and molecular mechanism. *Nature* **1991**, *349*, 117–127.
- (45) Schapira, M.; Abagyan, R.; Totrov, M. Nuclear hormone receptor targeted virtual screening. *J. Med. Chem.* **2003**, *46*, 3045–3059.
- (46) Civasotto, C. N.; Ortiz, M. A.; Abagyan, R. A.; Piedrafit, F. J. In silico identification of novel EGFR inhibitors with antiproliferative activity against cancer cells. *Bioorg. Med. Chem. Lett.* **2006**, *16*, 1969–1974.
- (47) Sever, S.; Muhlberg, A. B.; Schmid, S. L. Impairment of dynamin's GAP domain stimulates receptor-mediated endocytosis. *Nature* **1999**, *398*, 481–486.
- (48) Chen, H.; Lyne, P. D.; Giordanetto, F.; Lovell, T.; Li, J. On evaluating molecular docking methods for pose prediction and enrichment factors. *J. Chem. Inf. Model.* **2006**, *46*, 401–415.
- (49) Laskowski, R. A.; MacArthur, M. W.; Moss, D. S.; Thornton, J. M. PROCHECK: a program to check the stereochemical quality of protein structures. *J. Appl. Cryst.* **1993**, *26*, 283–291.
- (50) Reubold, T. F.; Eschenburg, S.; Becker, A.; Leonard, M.; Schmid, S. L.; Vallee, R. B.; Kull, F. J.; Manstein, D. J. Crystal structure of the GTPase domain of rat dynamin 1. *Proc. Natl. Acad. Sci. U.S.A.* **2005**, *102*, 13093–13098.
- (51) Lipinski, C. A.; Lombardo, F.; Dominy, B. W.; Feeney, P. J. Experimental and computational approaches to estimate solubility and permeability in drug discovery and development settings. *Adv. Drug Delivery Rev.* **2001**, *46*, 3–26.
- (52) Su, S.; Giguere, J. R.; Schaus, S. E.; Porco, J.; John, A. Synthesis of complex alkoxyamines using a polymer-supported *N*-hydroxyphthaladyn. *Tetrahedron* **2004**, *60*, 8645–8657.
- (53) Ferguson, S. M.; Brasnjo, G.; Hyashi, M.; Wolfel, M.; Collesi, C.; Giovedi, S.; Raimondi, A.; Gong, L. W.; Areil, P.; Paradise, S.; O'Toole, E.; Flavell, R.; Cremona, O.; Miesenbock, G.; Ryan, T. A.; De Camilli, P. A selective activity-dependent requirement for dynamin 1 in synaptic vesicle endocytosis. *Science* **2007**, *316*, 570–574.
- (54) Anggono, V.; Cousin, M. A.; Robinson, P. J. Styryl dye-based synaptic vesicle recycling assay in cultured cerebellar granule neurons. *Methods Mol. Biol.* **2008**, *457*, 333–345.
- (55) Chappie, J. S.; Acharya, S.; Leonard, M.; Schmid, S. L.; Dyda, F. G domain dimerization controls dynamin's assembly-stimulated GTPase activity. *Nature* **2010**, *465*, 435–440.
- (56) Davies, S. P.; Reddy, H.; Caivano, M.; Cohen, P. Specificity and mechanism of action of some commonly used protein kinase inhibitors. *Biochem. J.* **2000**, *351*, 95–105.
- (57) Massova, I.; Martin, P.; Bulychev, A.; Kocz, R.; Doyle, M.; Edwards, B. F. P.; Mobashery, S. Templates for design of inhibitors for serine proteases: application of the program dock to the discovery of novel inhibitors for thrombin. *Bioorg. Med. Chem. Lett.* **1998**, *8*, 2463–2466.